Applied Thermal Engineering 289 (2026) 129738

Contents lists available at ScienceDirect

Applied Thermal Engineering

journal homepage: www.elsevier.com/locate/apthermeng

Research Paper

Improving variable refrigerant flow system operation and energy efficiency: A study of the urban Minoh campus, Osaka, Japan

Toshihiro Suzuki [a,*], Yoshiyuki Shimoda [b], Shuta Matsuura [b], Sumio Shiochi [c]

[a] Campus Sustainability Office, Osaka University, Osaka, Japan
[b] Graduate School of Engineering, Osaka University, Osaka, Japan
[c] Technology and Innovation Center, Daikin Industries, Ltd., Osaka, Japan

ARTICLE INFO

Keywords:
Variable refrigerant flow
Energy efficiency
Energy management
Medium-sized building

ABSTRACT

Variable refrigerant flow (VRF) systems are widely adopted in commercial and institutional buildings; however, their actual performance often diverges from design expectations due to oversizing, low-load operation, and user-driven control behaviors. To clarify these issues and quantify their impact, this study conducts a comprehensive operational analysis of 100 outdoor units and 650 indoor units installed across a large multi-purpose academic building at Osaka University's Minoh Campus. One-year high-resolution operational data were examined to characterize part load ratios (PLRs), COP behavior, refrigerant-cycle conditions, and inefficiencies caused by excessive temperature settings, nighttime unattended operation, and uneven indoor-unit usage patterns. The analysis identified frequent low-load operation and oversized outdoor units as primary causes of performance degradation. After implementing operational energy-saving measures—including optimal temperature settings, reduced nighttime operation, and improved control awareness—the annual VRF energy use decreased by 12.9%. Additionally, a capacity optimization simulation revealed that resizing oversized outdoor units could yield a further 15.9% reduction, emphasizing the need to address both operational and design-level inefficiencies. The study demonstrates that substantial energy savings can be achieved through combined operational improvements and capacity optimization, even in large-scale, diverse-use campus buildings. These findings offer practical insights for enhancing VRF system performance and provide evidence-based guidance for improving energy management in buildings employing distributed air-conditioning systems.

1. Introduction

Global demand for air conditioning is increasing rapidly, and according to the International Energy Agency (IEA), the number of installed air-conditioning units is projected to triple by 2050 [1]. Because cooling systems already account for a substantial share of building energy consumption, this trend poses a serious challenge to achieving a carbon-neutral society. In particular, in commercial and educational buildings, air-conditioning systems play a crucial role in determining overall building energy performance.

In recent years, variable refrigerant flow (VRF) systems have been widely adopted, especially in Asia, owing to their flexible zoning capability, ease of installation, and relatively high efficiency under part-load operation. In theory, VRF systems can respond effectively to load variations and are therefore expected to achieve higher energy performance than conventional centralized air-conditioning systems.

A large number of studies on VRF systems have been conducted at the component and refrigerant-cycle levels. Research on compressor behavior, vapor–liquid refrigerant distribution characteristics, evaluation of alternative refrigerants, and short-term operating characteristics has been reported [2–15], contributing significantly to the understanding of VRF system mechanisms and their theoretical performance.

Through these studies, understanding of the fundamental behavior and performance characteristics of VRF systems has advanced considerably. However, these findings mainly focus on individual components, refrigerant-cycle behavior, or short-term operating conditions, and therefore do not directly reflect long-term operational behavior in real buildings under diverse usage conditions. In actual building operation, discrepancies between design assumptions and real loads, variability in operating conditions caused by user behavior, and prolonged low-load operation often coexist, resulting in energy performance that differs from theoretical expectations.

* Corresponding author.
E-mail address: suzuki.toshihiro.cso@osaka-u.ac.jp (T. Suzuki).

https://doi.org/10.1016/j.applthermaleng.2026.129738
Received 14 October 2025; Received in revised form 26 December 2025; Accepted 6 January 2026
Available online 20 January 2026

Against this background, despite their inherently high efficiency potential, VRF systems often exhibit significant operational inefficiencies in real buildings. Field investigations have repeatedly reported issues such as oversized system capacity relative to actual loads, persistent low part-load operation, and user-dependent control via remote controllers, leading to excessive temperature settings and unintended nighttime operation. Although these factors can substantially degrade system efficiency, their impact on energy performance has not been sufficiently quantified, particularly in large-scale, multi-purpose buildings.

Previous studies addressing operational issues of VRF systems can be broadly classified into several research domains. The first domain focuses on operational analysis and performance diagnosis, in which measured or calculated operational data are used to evaluate indicators such as the coefficient of performance (COP), seasonal energy efficiency ratio (SEER), operating time, and part-load ratio. For example, Zhang et al. [16] analyzed a VRF system with 16 indoor units in an office building and demonstrated that occupant behavior has a strong influence on energy consumption. Qian et al. [17] investigated 344 residential VRF systems and identified climate conditions, operating schedules, and system overcapacity as major contributors to efficiency degradation. Furthermore, Liu et al. [18] analyzed 16,985 residential VRF systems and showed that partial-load operation is common even in residential applications. Although several field studies have shown that occupant behavior and manual overrides significantly influence VRF energy consumption, most of them focus on aggregated energy use rather than examining how such user-driven operations translate into prolonged low-load operation, nighttime running, and COP degradation over long-term real-building operation. As a result, the operational consequences of user-driven overrides remain insufficiently quantified, especially in large multi-purpose buildings.

The second research domain concerns energy consumption prediction and modeling. Accurate prediction of energy consumption is essential for effective system management and fault detection. Zhou et al. [19] compared several neural network models and showed that multiple linear regression is effective for small datasets. He et al. [20] proposed a hybrid prediction model combining data partitioning and swarm intelligence algorithms, achieving high prediction accuracy.

The third research domain focuses on optimal control strategies, particularly model predictive control (MPC). Kang et al. [21] developed an MPC approach using neural networks, and Lee et al. [22] verified its effectiveness through experiments conducted in a real building. While these advanced control strategies address limitations of conventional VRF control logic, most of them are evaluated under limited experimental conditions or short-term demonstrations. As a result, how such control limitations manifest in long-term real-building operation, particularly in large multi-purpose facilities with strong user intervention, has not been sufficiently clarified.

In addition, studies on fault diagnosis and predictive maintenance, as well as cloud-based energy management services, have also progressed [23,24]. However, most of these studies focus on individual technologies or control methods, and few have comprehensively evaluated operational inefficiencies, improvement effects, and design implications based on long-term operational data from real buildings.

Based on this background, this study conducts a comprehensive evaluation of VRF system operation at the Osaka University Minoh Campus, which opened in 2021. Using one year of high-resolution operational data, we analyze part-load ratios, normalized COP behavior, temperature setpoint distributions, nighttime unattended operation, and variability in indoor-unit usage. Furthermore, the effectiveness of operational improvement measures implemented in the following year is evaluated, and a capacity optimization simulation is conducted for oversized outdoor units to quantify the potential for additional energy savings.

The main contributions of this study are as follows:

(1) providing one of the largest field-based evaluations of VRF performance in a multi-purpose university building;

(2) quantitatively demonstrating user-induced operational inefficiencies and the effectiveness of practical operational improvement measures; and.

(3) linking operational analysis results to design-level implications through capacity optimization.

The remainder of this paper is organized as follows. Section 2 describes the target building, the configuration of the VRF system, the data collection methods, and the evaluation metrics used in this study. Section 3 presents the results of the operational analysis based on real operating data, including the relationship between part-load ratio and COP, user-induced operational inefficiencies, the effectiveness of energy-saving measures, and the results of the capacity optimization analysis. Finally, Section 4 summarizes the main findings of this study and discusses their implications for improving VRF system operation and design in real buildings.

2. Methods

2.1. Building outline

This study focuses on the Osaka University Foreign Language Research and Lecture Building (Minoh Campus, Osaka, Japan), which commenced operation in the 2021 academic year and serves as the new campus for Osaka University's Faculty of Foreign Studies. Various facilities were consolidated within a single 10-story building with a total floor area of approximately 25,000 m^2. The exterior of the building is shown in Fig. 1. Although the building is equipped with VRF systems similar to those in urban office buildings, its use as a university campus makes it distinct. An outline of the Minoh Campus is shown in Fig. 2. The first floor contains large halls and lecture rooms; the second floor is primarily allocated to offices; the third floor houses a piloti and connects to the exterior and a cafeteria; the fourth through seventh floors feature lecture rooms and student common spaces used by a large number of people; and the eighth through tenth floors are predominantly occupied by faculty offices. No notable structural differences were observed among the upper floors.

Because the facility is a university building, extended holidays during the summer and winter result in user trends that differ markedly from those in typical office buildings.

2.2. Outline of VRF system

At the Minoh Campus, 100 outdoor units (OUs) and 650 indoor units (IUs) have been installed (Fig. 2). Although the floor areas are identical, the number of installed VRF systems varies. Floors 6–7 and 8–10 have nearly identical room functions and layouts, resulting in similar VRF system configurations. Floors 4 and 5 contain more VRF systems because

Fig. 1. Exterior view of the Minoh campus.

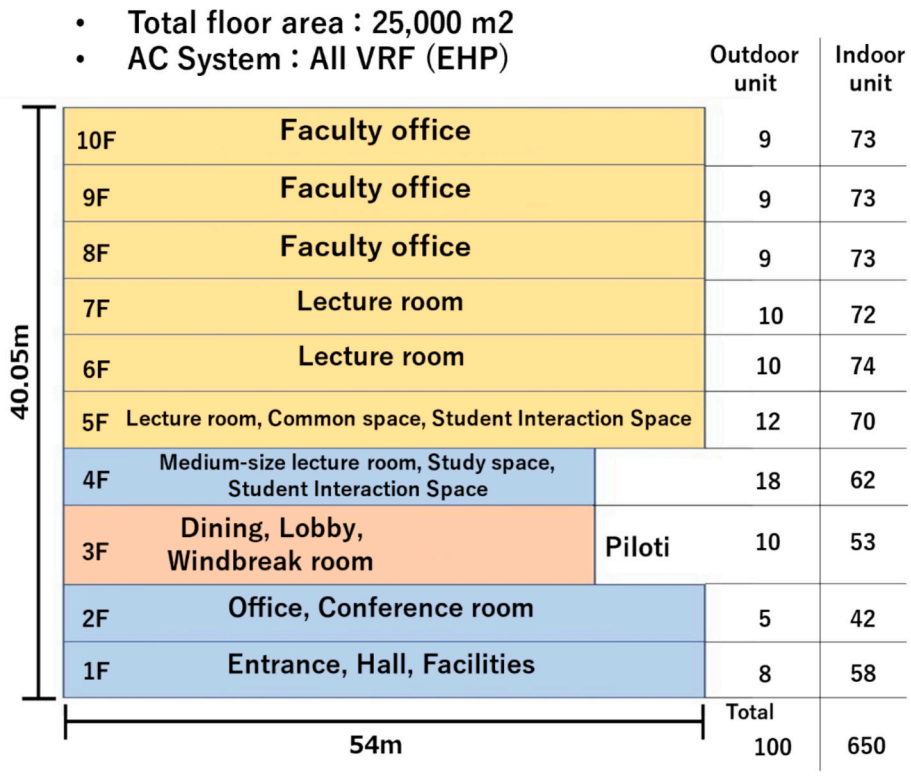

Fig. 2. Outline of the Minoh campus.

they include multiple rooms with different functions, such as common spaces and server rooms, in addition to lecture rooms. Moreover, Floors 1 and 2 have fewer VRF systems due to the reduced number of rooms compared to the upper floors.

2.3. Sensing framework outline

Section 2.3 describes the data acquisition and storage framework used to collect operational information from the air-conditioning systems at the Minoh Campus. An overview of this framework is shown in Fig. 3.

At the Minoh Campus, indoor units (IUs) and outdoor units (OUs) within the same VRF system are directly connected via a communication line to a central air-conditioning controller. Operational data are transmitted from this central controller to a cloud-based storage system via mobile communication devices. The data stored through this framework are limited to the control-related information available from sensors originally installed by the manufacturer for equipment operation, such as temperature and pressure sensors. Other types of data are not available within this monitoring framework. The stored cloud data are subsequently downloaded to a local analysis computer, enabling offline data processing and analysis [25]. Details of the operational data obtained from the indoor units and outdoor units are described in Section 2.4. In addition, as shown in Fig. 3, the Minoh Campus is equipped with a separate electricity metering system that measures power consumption related to lighting, electrical outlets, and air-conditioning equipment. A total of 270 watt-hour meters are installed across the campus, and the corresponding electricity consumption data are transmitted to a server via an independent mobile communication network.

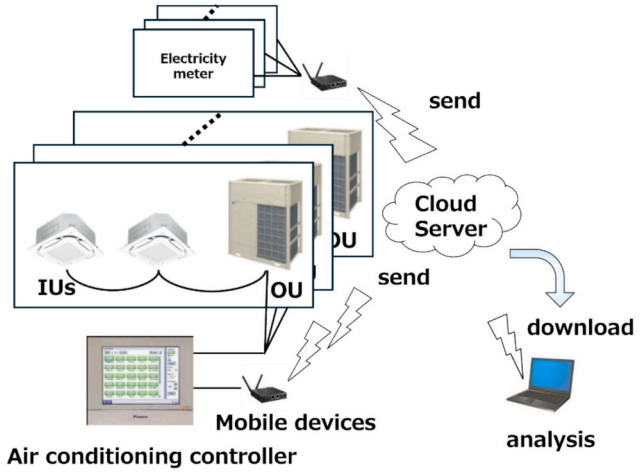

Fig. 3. Sensing framework of the Minoh campus.

2.4. VRF system operational data

This section describes the operational data obtained from the VRF systems and used for the subsequent analyses. The data were collected from the remote monitoring system installed at the Minoh Campus and consist of time-series records from both outdoor units (OUs) and indoor units (IUs). These data were originally recorded for maintenance and operational management purposes and were directly utilized in this study without additional filtering or gap-filling.

The operational parameters available from the monitoring system include equipment operating states, thermal performance indicators, and energy-related variables. All data are stored at a fixed hourly resolution, enabling consistent long-term analysis of system behavior. The specific parameters used in this study are summarized in Table 1. The output data from the OUs include: the operation mode, indicating the operational state of cooling, heating, or fan mode; operation time, representing the operating duration within 1 h; cooling/heating capacity denoting the accumulated capacity over 1 h (see Section 2.5); cooling/heating PLR representing the average 1-h PLR during cooling/heating; cooling/heating coefficient of performance (COP), representing the

Table 1
Operational parameters.

	Parameters	Period/ Interval
Outdoor units (OUs)	Operation mode OU operation time Cooling processing capacity Heating processing capacity Cooling PLR Heating PLR Cooling COP Heating COP Energy consumption	April 1, 2021 - March 31, 2023 / 1 h
Indoor units (IUs)	Average Set temperature Average Suction temperature IU operation time Thermo-on time	

average COP over 1 h of cooling/heating; and energy consumption, indicating the accumulated energy consumed over 1 h.

Similarly, the output data from the IUs include: the time-averaged set temperature; suction temperature, providing a 1-h average measured at the suction port of the IU; operation time, indicating the operating duration; and Thermo-on time, reflecting the duration of the IU's thermo-on state.

2.5. Cooling and heating capacity

The cooling and heating capacities were calculated using the compressor curve (CC) method, a type of refrigerant enthalpy method [26]. The CC method is a capacity calculation approach that considers actual operational information, refrigerant flow defined by the compressor performance curve, and the refrigerant enthalpy difference in the connection piping between the IU and OU. The cooling capacity (Qc) is determined by multiplying the IU refrigerant flow (G) by the refrigerant enthalpy difference (Δi) and then subtracting the IU fan power (Wi) (Eq. 1). Conversely, the heating capacity (Qh) is obtained by adding the IU fan power (Wi) to the product of the IU refrigerant flow (G) and the refrigerant enthalpy difference (Δi) (Eq. 2).

In cooling mode, the electrical losses of the indoor fan motor appear as sensible heat added to the conditioned space, which the cooling coil must remove. Therefore, fan power is subtracted to obtain the net cooling capacity delivered to the space. In contrast, during heating mode, the fan motor heat contributes directly to indoor sensible heating, and thus it is added to the gross heating capacity to calculate the net heating capacity. This treatment is consistent with conventional HVAC thermodynamic practice.

$$Qc = \Delta i \times G - Wi \tag{1}$$

$$Qh = \Delta i \times G + Wi \tag{2}$$

The average PLR was calculated using Eq. 3, which uses the hourly air-conditioning capacity (Q^{VRF}) obtained via the CC method and the rated capacity (Q) of the equipment. The COP was computed using Eq. 4, based on the air-conditioning capacity (Q^{VRF}) and OU power consumption (P) during the target period. In the case of COP, it is necessary to evaluate whether the equipment is demonstrating its inherent performance characteristics. Therefore, we evaluated it using the normalized COP (Eq. 5), which is calculated by dividing the measured COP by the rated COP provided by the manufacturer.

$$u = \frac{Q^{VRF}}{Q} \tag{3}$$

$$COP = \frac{Q^{VRF}}{P} \tag{4}$$

$$Normalized\ COP = \frac{COP}{Rated\ COP} \tag{5}$$

2.6. Compressor-on ratio of IU

To evaluate the duration for which the IU is operating, the following Compressor-on ratio of the IU was defined and evaluated. The compressor-on ratio Ri for OU i is defined as:

$$R_i = \frac{\sum (CI_k \times t^*_k)}{CO_i \times t_i} \tag{6}$$

Here, CI_k is the rated capacity of IU k, CO_i is the rated capacity of OU i, t_i is the operating time of OU i, and t^*_k is the thermo-on operating time of IU k.

2.7. Schematic layout of three representative systems

Given the large number of VRF systems installed in the building, three representative systems were selected for detailed specification and layout analysis. The representative systems were selected to capture the diversity of space usage, control configurations, and part-load operating characteristics observed in the building.

Figs. 4–6 show the indoor layouts of the three outdoor unit systems used as representative systems for the operational analysis in Section 3.3. As shown in Fig. 4, five IUs were installed in the interaction space and operated via a single remote control. In contrast, Figs. 5 and 6 illustrate the layouts of the lecture rooms and faculty offices, where one remote control was installed in each room, enabling operation on a per-room basis.

Information on the air-conditioning units is presented in Table 2. Both systems use ceiling-mounted cassette-type IUs with low fan power. The table also shows the capacity ratio of the connected IUs. The OU was designed with a low connection capacity ratio to compensate for the piping length resulting from its installation on the rooftop.

3. Results and discussion

3.1. Evaluation of 100 VRF systems using annual average operational data

In this section, the physical quantities affecting the annual average normalized COP of each of the 100 VRF systems were investigated using one year of operating data, from April 2021 to March 2022. Specifically, the effects on the normalized COP were analyzed for the average annual PLR, average annual setpoint temperature, average annual operating hours, and average annual compressor-on ratio of the IUs.

3.1.1. PLR relative to normalized COP

First, the average cooling and heating PLRs and normalized COPs for all 100 OU systems were analyzed. The scatter plot for cooling is presented in Fig. 7. Colors were assigned according to usage; for example, common spaces are depicted in red and cafeterias in blue.

Fig. 7 shows several distinctive cooling characteristics. The highest average COP was observed in the server room, plotted in black on the upper left. Presumably, the implementation of a high sensible heat mode for server applications resulted in efficient operation. Operation during periods of lower outdoor temperatures, owing to year-round cooling, contributed to the elevated average COP. Excluding the server room, the

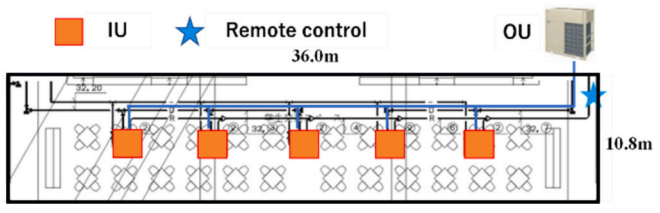

Fig. 4. Schematic layout of 5th-floor interaction space.

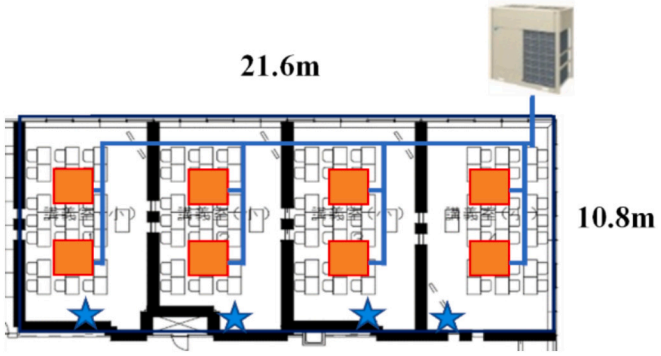

Fig. 5. Schematic layout of 5th-floor lecture room.

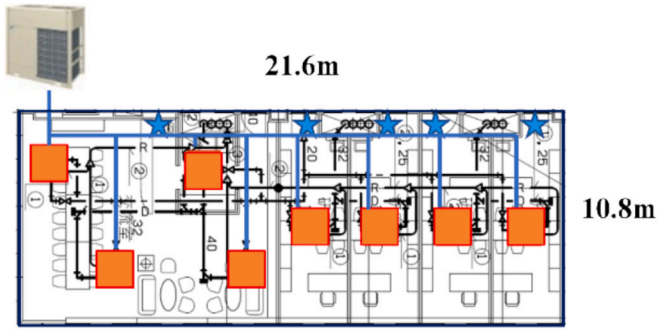

Fig. 6. Schematic layout of the 10th-floor faculty office.

highest average COP was noted for the 5th-floor interaction space (normalized COP = 1.13, PLR = 0.39). Common-space usage exhibited relatively high PLRs and COP. Notably, the system with the highest PLR was the middle lecture room. Although two OUs were installed in the middle lecture room, only one system was prioritized for operation during the intermediate period according to the schedule, resulting in a high PLR. Following the common space, cafeteria usage (depicted in blue) displayed the next highest PLR and COP, likely owing to the substantial load during lunchtime. In contrast, lecture room usage (in green) shows annual average PLRs of around 0.10; however, the hourly PLR distribution includes many operating periods near PLR ≈ 0.3, where COP remains relatively high. As a result, the average normalized COP stays around 0.75, indicating that a PLR of 0.10 does not necessarily lead to a significant reduction in COP as demonstrated in Fig. 15.

Conversely, faculty office usage (in purple) exhibited an even lower annual average PLR of approximately 0.05. Under such extremely low-load conditions, the compressor frequently cycles between start and stop, causing a substantial reduction in COP.

Correlation coefficients were calculated to confirm the relationship between PLR and normalized COP (excluding the server room system, which is used as a year-round cooling system). The coefficient of determination was 0.48, and the RMSE (root mean square error) was 0.12. In the case of cooling, it was confirmed that there was a moderate degree of correlation, although significant variation was present.

Fig. 8 indicates that, similar to the cooling operation, common space usage exhibits both high PLRs and COP during heating. For the other systems, the relationship between PLR and normalized COP showed the same trend as in cooling. The coefficient of determination was 0.71, and the RMSE was 0.09, indicating a stronger correlation for heating than for cooling.

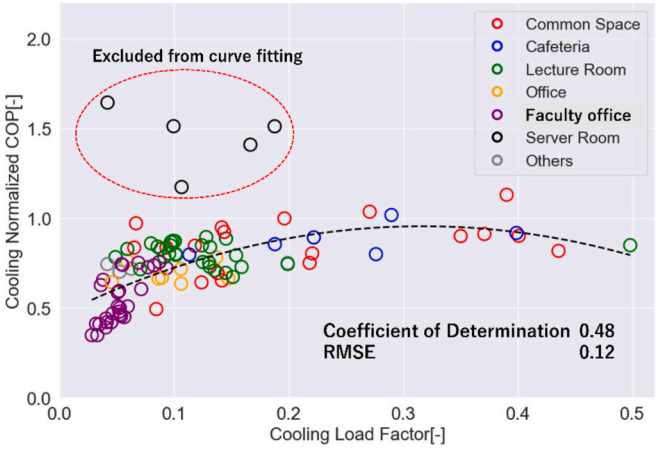

Fig. 7. Relationship between average PLR and average normalized COP associated with cooling operation.

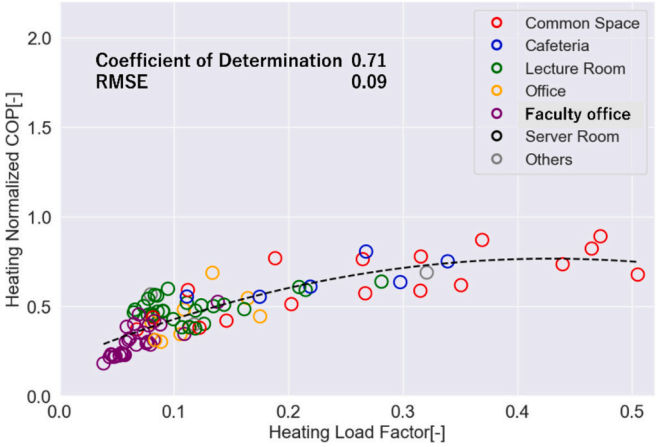

Fig. 8. Relationship between average PLR and average normalized COP associated with heating operation.

Table 2
Air conditioner information.

Room name (	OU			IU		
	Rated cooling capacity (kW) / (IU connection capacity ratio)	Number of compressors	Rated COP (cooling/ heating)	IU type	Rated cooling capacity (kW)	Number of units
5th floor interaction space	56/(80%)	2	3.57/3.82	4-way cassette type	9.0	5
5th floor lecture room	50/(76%)	2	3.82/4.03	4-way cassette type	4.5	6
					5.6	2
10th floor faculty office	40/(81%)	1	3.74/4.13	2-way cassette type	3.6	4
				4-way cassette type	4.5	4

The relatively low average PLRs (generally below 0.5) can be attributed to the operational characteristics of the campus buildings. In multi-purpose facilities such as classrooms and faculty offices, air-conditioning demand is intermittent, with units often operating at low PLRs or remaining idle for extended periods. Consequently, simultaneous full-load operation of all connected indoor units rarely occurs. Our findings confirm that low PLRs are a typical characteristic of VRF operation in real-world buildings, especially in large-scale, multi-use buildings.

3.1.2. Set temperature relative to normalized COP

Next, the relationship between the temperature setting of each IU and the normalized COP was investigated. The results are shown in Fig. 9. For example, in the case of cooling, raising the temperature setting theoretically reduces the load, resulting in lower energy consumption. However, it is clear from Fig. 9 that the normalized COP, which indicates efficiency even when the temperature setting is increased, shows considerable variation in both cooling and heating, regardless of the application. The coefficient of determination and the RMSE for cooling were 0.19 and 0.21, respectively. Those for heating were 0.06 and 0.16, respectively. The correlations were low for both cooling and heating. In particular, no correlation with normalized COP was observed for common space and faculty room applications, despite the large variation in temperature settings.

3.1.3. Runtime relative to normalized COP

Next, the relationship between the normalized COP and the runtime of each IU (Fig. 10) was investigated. As is clear from the figures, the coefficient of determination and root-mean-square error for cooling were 0.13 and 0.21, respectively, while those for heating were 0.06 and 0.16, indicating a low correlation. It can be concluded that runtime, whether short or long, has little impact on normalized COP.

3.1.4. Compressor-on ratio of IU relative to normalized COP

Finally, a comparison was made between the compressor-on ratio of the IU and the normalized COP (Fig. 11). Similar to the PLR, the normalized COP tended to be higher when the compressor-on ratio of the IU was higher. The coefficient of determination and RMSE for cooling were 0.49 and 0.15, respectively—values similar to those for the PLR and normalized COP. For heating, the values were 0.48 and 0.12, which were slightly lower than those for the PLR. The compressor-on ratio of the IU indicates the percentage of IUs connected to each system that are operating simultaneously. This value does not count when users intentionally do not operate individual IUs or when IUs are operating but are in a thermo-off state, meaning there is no load to process in the room. Therefore, to increase the compressor-on ratio of the IU, all IUs connected to the OU must be operating simultaneously and generating a steady load. The results indicate that improving the normalized COP, which reflects the efficiency of the air conditioner, requires increasing the ratio of IU use. In the scatter plots of PLR and normalized COP, the server room system was an outlier with a large deviation from the overall trend, but the compressor-on ratio of the indoor units showed the same trend as the other systems. It was confirmed that the compressor-on ratio of the indoor units is also an important indicator for explaining normalized COP. The normalized COP shown in this study is based solely on outdoor-unit power consumption (Eq. (4)), and therefore indoor-unit fan electricity is not included. Recent VRF systems mitigate unnecessary increases in total power consumption by reducing indoor-fan airflow after the set temperature is reached, contributing to lower overall energy use.

3.2. Analysis results for hourly PLR

Next, we evaluated the frequency distribution of the load factor, previously shown to have the highest correlation with normalized COP, in each system. To facilitate intuitive understanding, we used a violin plot for evaluation (Figs. 12 and 13). Fig. 12, which presents the cooling results, shows all 100 OU results ordered by the highest average annual normalized COP. The X-axis shows the OU number. The top three are server rooms, as mentioned above, but they operate with a low load factor of about 0.2. The low PLR (≈0.2) of the server rooms is primarily due to the installed VRF capacity being larger than the actual heat generation of the servers. The rooms require cooling throughout the entire year, and during winter the sensible heat load becomes even smaller, leading to a further reduction in load factor. The next highest-ranked OUs are interaction spaces. It is also evident that their distribution resembles a “vase” shape, extending from high to low PLRs. These results confirm that the wide distribution of PLRs, from high to low, is the reason for the high COP values. On the other hand, the OUs in the lecture rooms, shown in green, appear in the middle of the overall ranking. Their distribution has few areas with high PLRs and exhibits a “bell-shaped” pattern, with PLRs concentrated around 0.1 to 0.3. Finally, the OUs with the lowest COP are concentrated in the faculty offices, shown in purple. Their distribution resembles a “pyramid” shape with a wider area at lower PLRs. These results indicate that the most efficient operation tends to follow this pattern: “vase-shaped” > “bell-shaped” > “pyramid-shaped.”

Similarly, a violin plot based on the PLR during heating is shown in Fig. 13. This confirms that the systems with the highest normalized COP are shared spaces, as in cooling, and their distribution is also “vase-

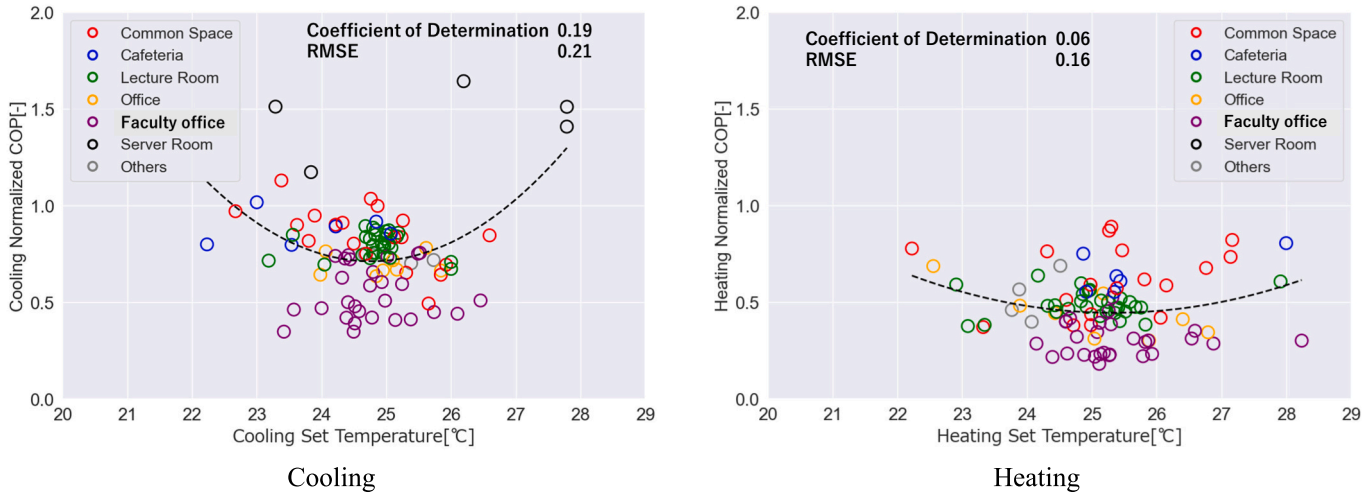

Fig. 9. Relationship between average set temperature and average normalized COP.

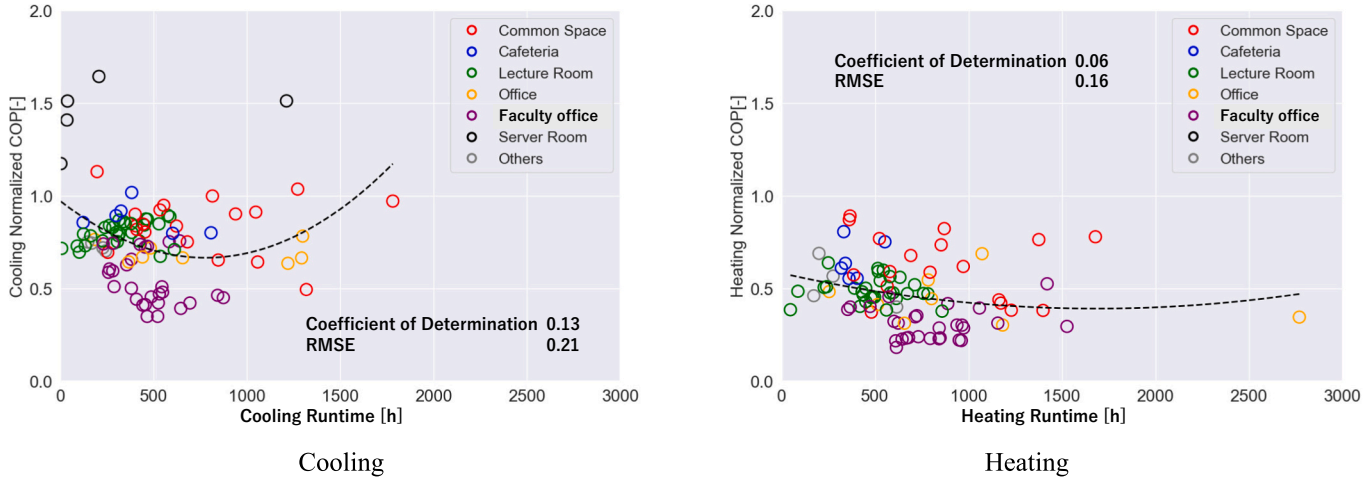

Fig. 10. Relationship between runtime and average normalized COP.

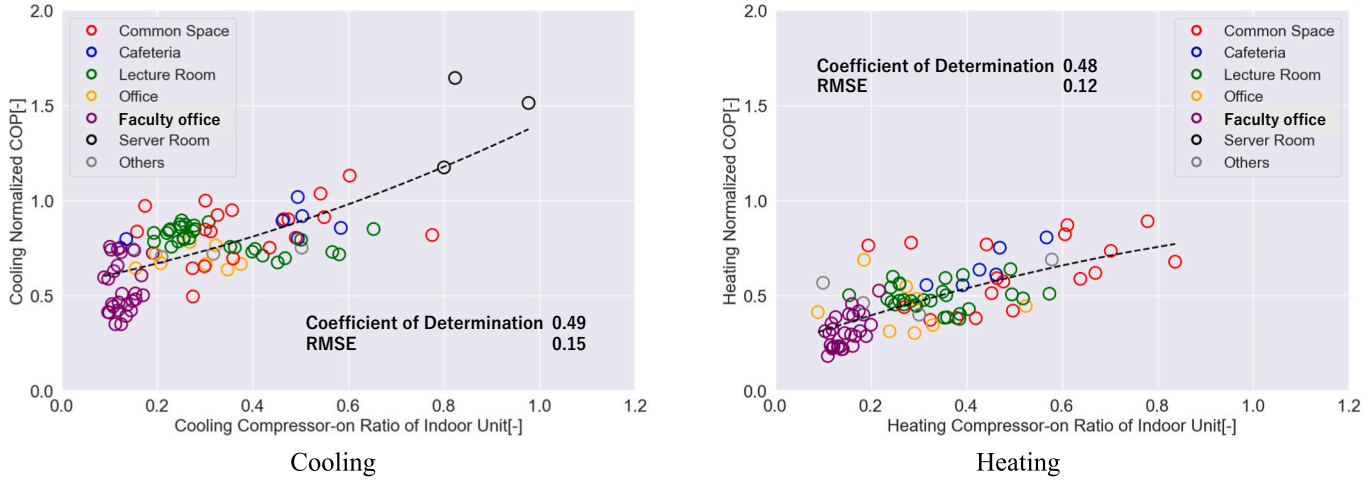

Fig. 11. Relationship between the average compressor-on ratio of IU and the average normalized COP.

shaped." The systems with the lowest normalized COP exhibit a "pyramid-shaped" distribution similar to that in cooling. These results demonstrate that violin plots can be used to intuitively evaluate load distribution.

3.3. *Detailed evaluation results of representative systems*

These findings indicate that the actual operation of VRF systems varies considerably depending on their use for both cooling and heating. Therefore, three representative systems were selected for a case analysis of air-conditioning operation. First, we examined the 5th-floor interaction space (Fig. 4), which showed the highest normalized COP, excluding the server system. Second, we analyzed the 5th-floor lecture room (Fig. 5), which had average values of PLR and normalized COP. Third, we evaluated the 10th-floor faculty office, which had the lowest PLR and normalized COP.

Figs. 14–16 illustrate the relationship between PLR and normalized COP during cooling for these three systems. The 5th-floor interaction space exhibited relatively uniform PLRs (average = 0.39), higher than those of the other systems. At a given PLR, lower outdoor temperatures (blue plots) were associated with higher normalized COPs, whereas higher outdoor temperatures (red plots) tended to result in lower normalized COPs. The PLR increased with rising outdoor temperature. The interaction space system demonstrated a uniform load distribution centered around a PLR of approximately 0.20 (red circle in Fig. 14), leading to a high average normalized COP (1.13). In contrast, the 5th-floor lecture room exhibited both lower PLRs and normalized COPs. The PLR in the 10th-floor faculty office was extremely low (average ≈ 0.04). Consequently, the OUs underwent frequent start–stop cycling, and the average normalized COP decreased to as low as 0.32.

Fig. 17 shows the frequency distribution of cooling set temperatures for the three systems. The set temperatures varied widely among users, who were free to adjust them. However, the high PLR observed in the interaction space, which had the highest average set temperature (25.0 °C), and the extremely low PLR in the 10th-floor faculty office, which had the lowest average set temperature (23.3 °C), cannot be explained solely by temperature settings. Therefore, the set temperature alone is insufficient to explain the relationship between PLR and normalized COP.

Fig. 18 illustrates the number of IUs operating concurrently during the first year. In the interaction space, five IUs were installed in an open area without partitions and controlled by a single remote control, resulting in all five units operating simultaneously. In the 5th-floor lecture room, dispersed rooms and concentrated lecture times led to an average of 4.3 IUs operating concurrently. In the 10th-floor faculty office, only one IU typically operated at a time, with an average of 1.6 active units.

Recent VRF systems tend to operate most efficiently when all

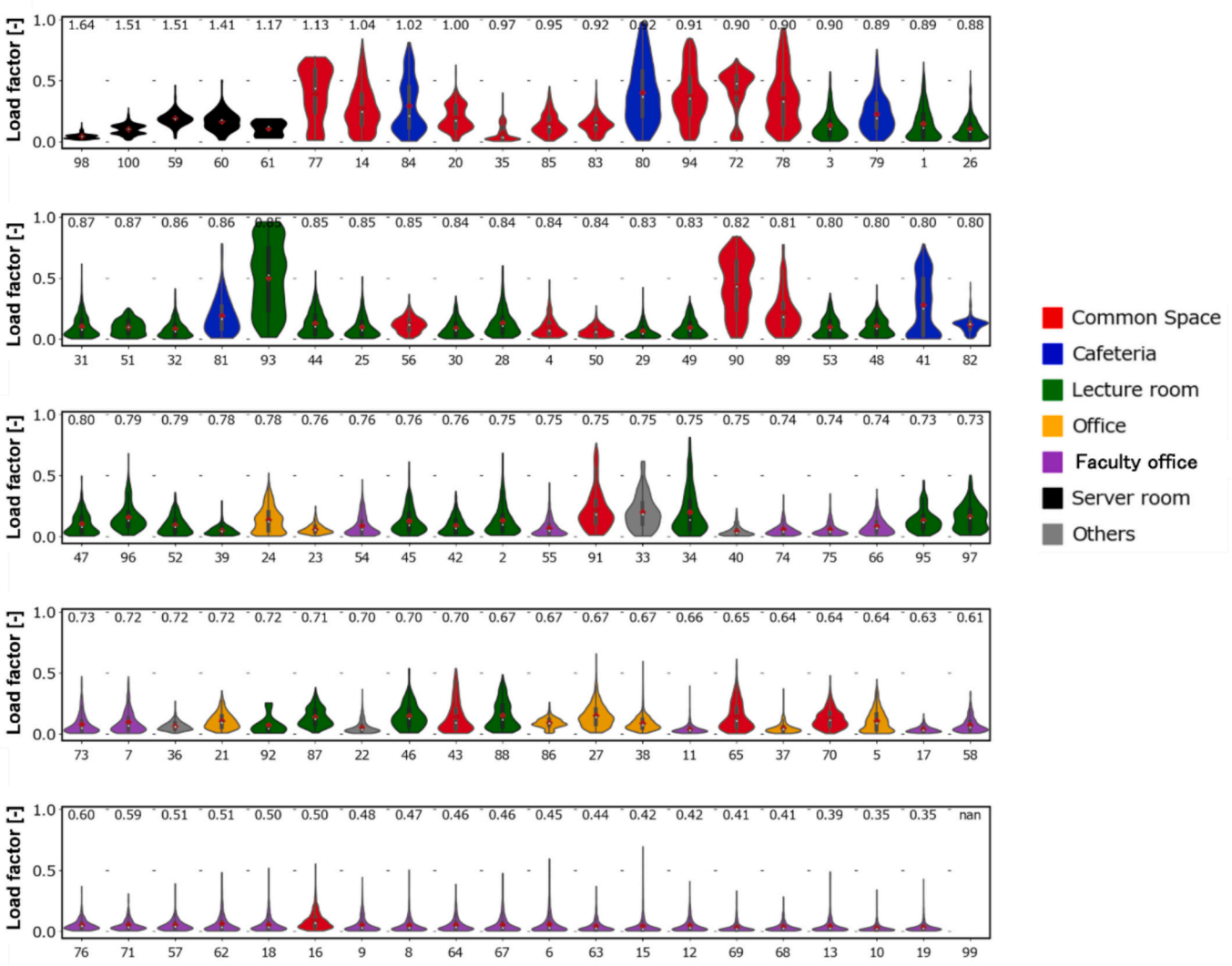

Fig. 12. Violin diagram based on PLR with cooling operation.

connected IUs run simultaneously and the PLR remains between 0.20 and 0.60. In contrast, efficiency declines when only a few IUs are active and is further reduced when low PLRs cause repeated start–stop cycling of the compressor. The 10th-floor faculty office exhibited both conditions, resulting in a very low COP.

The frequency distribution of evaporation temperatures during this period is shown in Fig. 19. In the 5th-floor interaction space, which had a high PLR and concurrent IU use, the average evaporation temperature was 7.4 °C. In the 5th-floor lecture room, which had a moderate PLR, the average evaporation temperature was 6.8 °C. In the 10th-floor faculty office, which had the lowest PLR and lowest concurrency, the average evaporation temperature was even lower at 5.7 °C.

In recent years, VRF has adopted a control method that raises the evaporation temperature in the medium load range to save energy and improve COP. Specifically, in the medium load range, the compressor speed is lowered to reduce the refrigerant flow rate, raising the evaporation temperature and improving the efficiency of the refrigerant cycle. However, when the PLR is insufficient or the concurrency of IU operation is low, the evaporation temperature does not rise, and system performance cannot be fully utilized. To address this issue, it is important to optimize OU capacity according to IU usage conditions.

3.4. Implementation and effectiveness of energy conservation measures

Two operational issues were identified during the initial year. The first was excessive set temperatures. Fig. 20 presents the distribution of the set cooling and heating temperatures for all VRF systems at the Minoh Campus during the initial year. The Ministry of the Environment in Japan recommends indoor temperatures of 28 °C in summer and 20 °C in winter. Operations at temperatures above the recommended value during cooling and below the recommended value during heating accounted for only about 5% of overall operations. However, there were frequent instances of operation at clearly excessive temperatures—for example, 20 °C during cooling and 30 °C during heating—leading to an increased processing load and, consequently, increased energy consumption.

The second issue pertained to unattended operation during late night and early morning. Fig. 21 presents the hourly OU operation time during the initial year, revealing that approximately 10% of operations occurred between 22:00 and 07:00, a period during which student access is restricted at the Minoh Campus. Consequently, the unintended operation of air conditioning during late night and early morning is another major operational challenge.

Two energy conservation measures (Table 3) were implemented to address these issues. Their effects on energy consumption were evaluated by comparing changes before (January–December 2022) and after

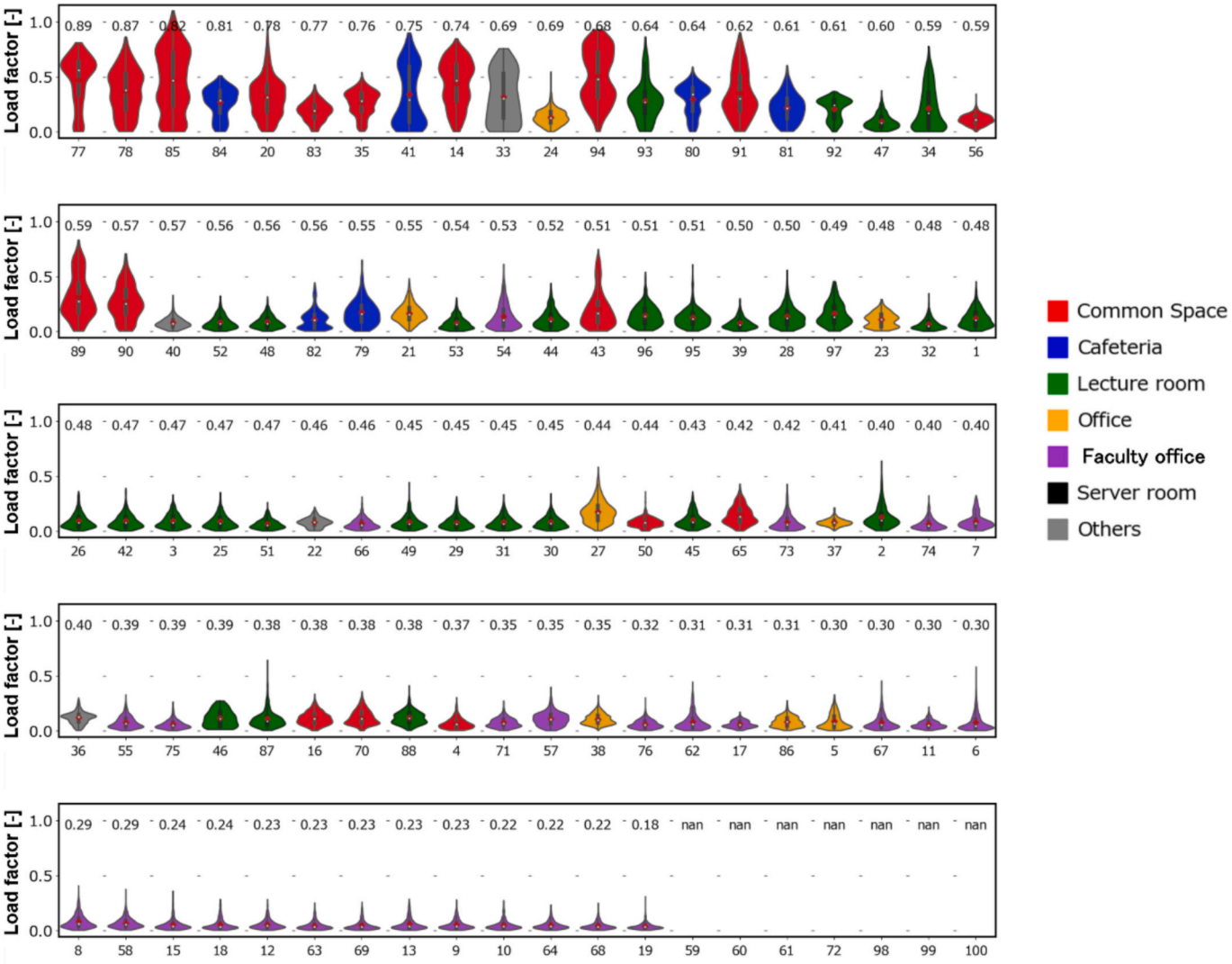

Fig. 13. Violin diagram based on PLR with heating operation.

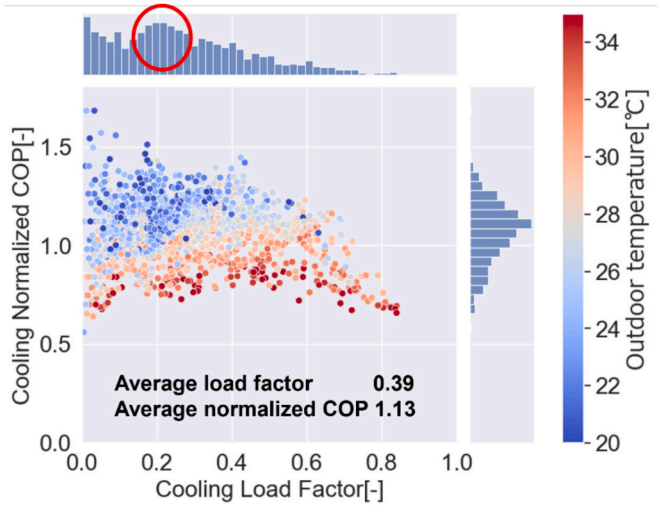

Fig. 14. Relationship between PLR and COP for the 5th floor interaction space.

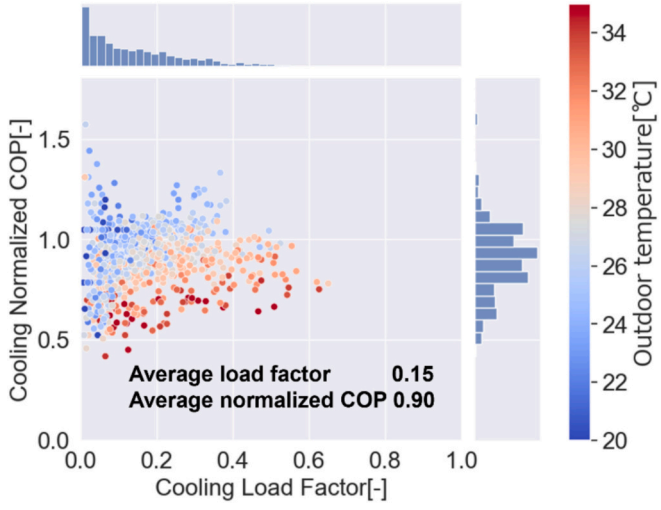

Fig. 15. Relationship between PLR and COP for the 5th-floor lecture room.

(January–December 2023) implementation. However, these measures targeted only 82 systems (hereafter called "all systems"), excluding those in server rooms and similar areas, out of a total of 100 systems.

Fig. 22 shows the distribution of set temperatures after the measures

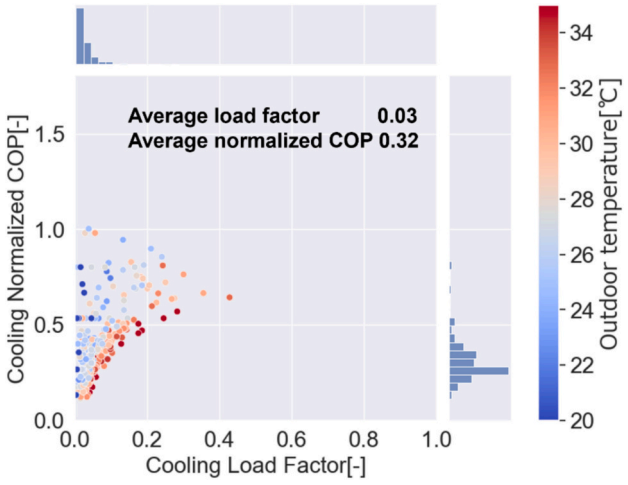

Fig. 16. Relationship between PLR and COP for the 10th faculty office.

were implemented. For cooling, the set temperatures were restricted to ≥25 °C, which helped prevent unnecessary operation. Similarly, for heating, the operation was maintained at ≤25 °C. However, in some cases, controlled release related to events was observed. In Japan, typical comfort setpoints are approximately 26 °C for cooling and 22–24 °C for heating. The modifications introduced in this study were limited to preventing excessively low cooling settings (e.g., below 24 °C) and excessively high heating settings (e.g., above 26 °C). Therefore, the implemented measures remained within widely accepted comfort ranges, and occupant comfort was not considered to be significantly affected.

Fig. 23 shows the hourly OU operation times before and after the

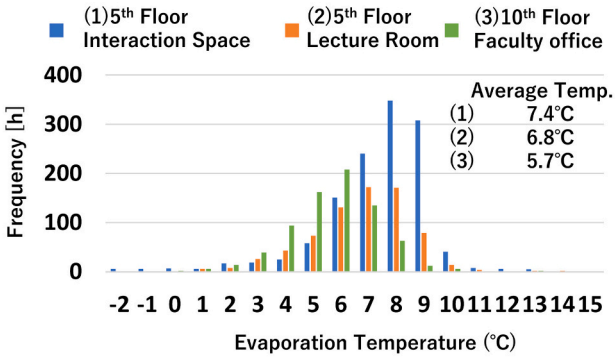

Fig. 19. Frequency distribution for evaporation temperature according to the facility.

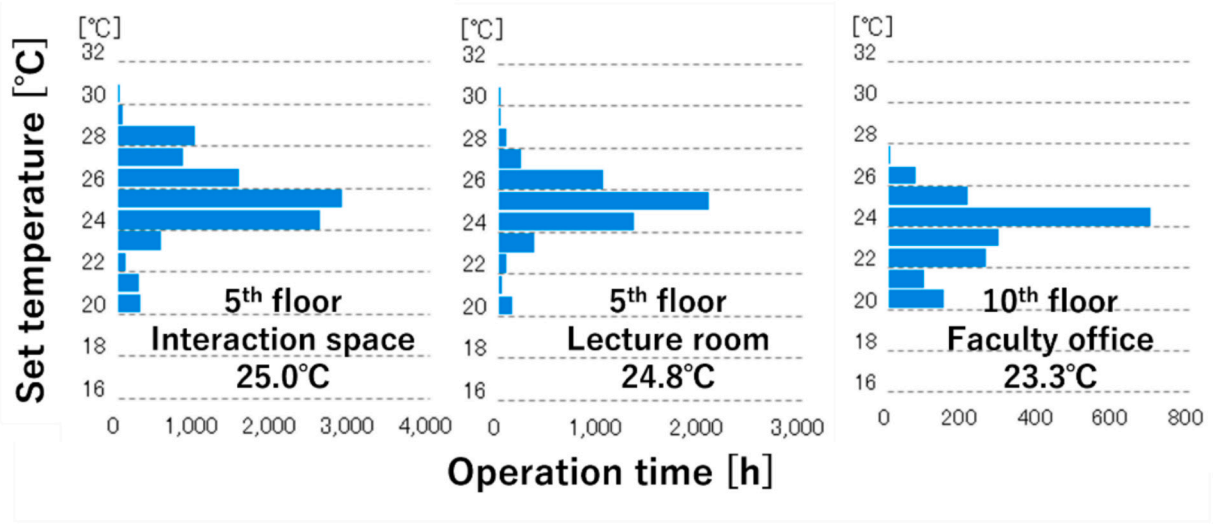

Fig. 17. Frequency distribution of cooling-set temperature.

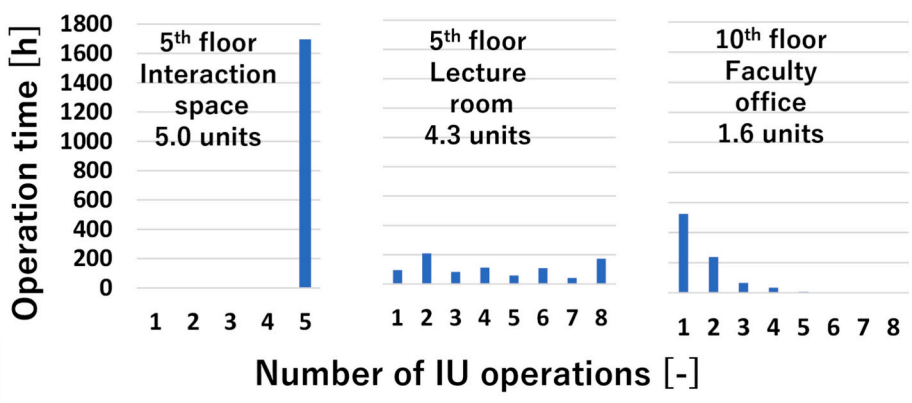

Fig. 18. Number of concurrent active IUs.

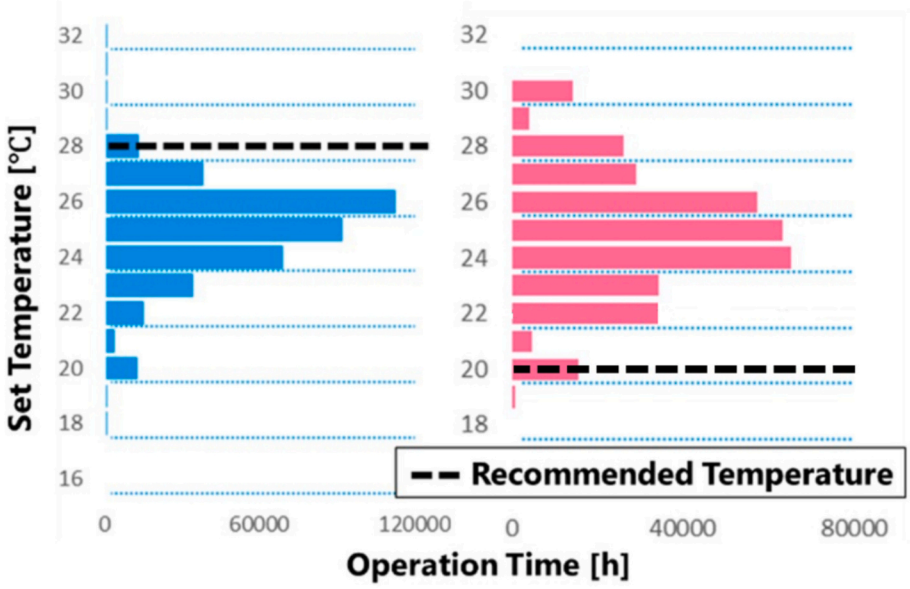

Fig. 20. Frequency distribution of set temperatures.

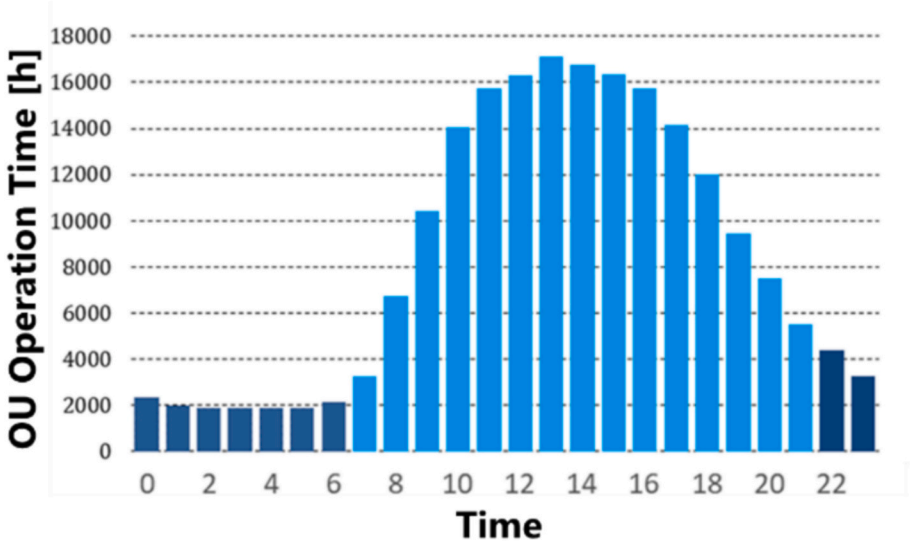

Fig. 21. OU operation time.

Table 3
Details of energy conservation measures.

	Details	Target systems
Set temperature restriction	Cooling min. 25 °C Heating max. 25 °C	82 systems, excluding server rooms, etc. (All systems)
Oversight control	Turn off IU at 22:00	

implementation of the measures. Nighttime operations were reduced by approximately 54% due to oversight control, and nighttime energy consumption was reduced by approximately 60%. However, the data indicated that after an air-conditioning system had been stopped once at 22:00, it was restarted and continued to operate until the morning. Currently, a stop command is issued at 22:00, but it appears that multiple stop commands at 00:00, 02:00, etc., are required. In addition, the increased operation time after 15:00 in 2023 is attributed to the cafeteria returning to its normal operating schedule following the end of COVID-19 restrictions. During 2022, the cafeteria operated with shortened hours, but in 2023, extended opening hours resulted in higher occupancy and increased thermal loads in the late afternoon.

To further clarify the nighttime operation shown in Fig. 23, Table 4 summarizes the rooms in which HVAC systems continued operating during nighttime hours, classified by space usage. The results indicate that nighttime unintended operation occurred most frequently in guard rooms and collaboration spaces. These spaces are often used intermittently at night or lack a clearly defined end time of occupancy, which likely increases the probability that HVAC systems remain in operation after use. In contrast, nighttime operation was also observed in some lecture rooms and laboratories; however, the frequency was relatively low compared with that in guard rooms and collaboration spaces. A comparison between weekdays and weekends was also conducted for nighttime operation, but no clear differences were observed. This suggests that nighttime unintended operation is not strongly dependent on the day of the week, but is instead closely related to space usage and

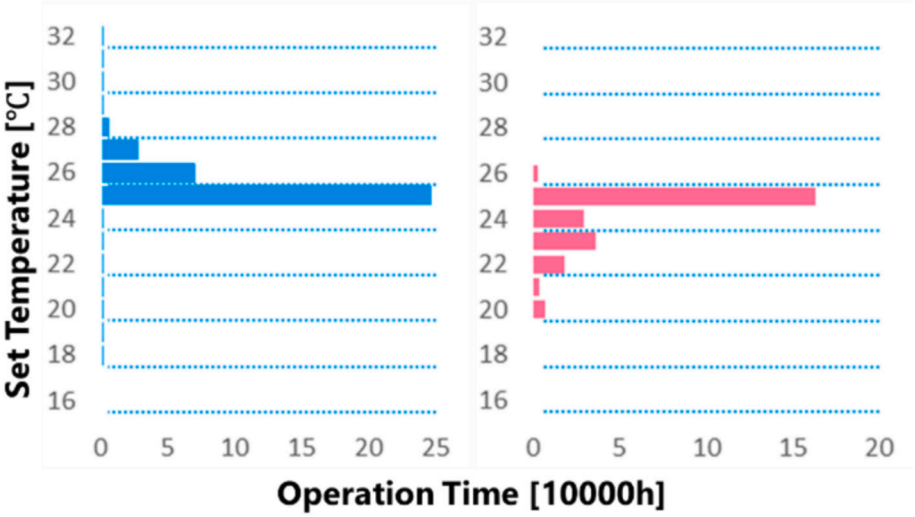

Fig. 22. Frequency distribution of set temperature for all systems.

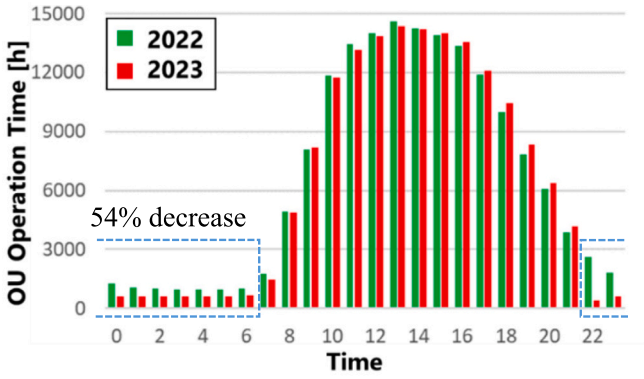

Fig. 23. Change in OU operation time for all systems.

Table 4
Breakdown of nighttime HVAC operation by space usage.

Space usage / Room type	Nighttime operating hours [h]
Guard room	2088
5th-floor interaction space	549
4th-floor interaction space	546
5th-floor laboratories	355
6th-floor interaction space	291
Others	514
Total	4342

occupancy characteristics. User behavior clustering analysis was not performed in this study. However, clustering based on operational and control histories could provide deeper insight into behavioral patterns associated with nighttime operation, and is therefore identified as an important topic for future research. Finally, it should be noted that all rooms on the campus are equipped with remote controllers, allowing users to freely start, stop, and adjust HVAC settings. This high level of user control is considered an important contextual factor influencing the observed nighttime operational behavior.

Fig. 24 shows the monthly air-conditioning energy consumption for all systems before and after the implementation of the measures. The annual energy consumption was 361 MWh in 2022 and 305 MWh in 2023, corresponding to a 15.4% consumption.

However, Fig. 24 does not account for the effect of outdoor temperature. To eliminate this effect, an outdoor temperature correction simulation was performed (see Appendix A Table A1).

The energy consumption of all systems was simulated for 2022 and 2023 (Table 5). Overall air-conditioning energy consumption decreased by 15.4% before temperature correction and by 12.9% after correction, compared with 2022. With only operational improvements as soft measures, an energy-saving effect of 12.9% was achieved.

However, the increased energy use observed in November 2023 was primarily due to significantly lower outdoor air temperatures compared with November 2022. The colder conditions increased the heating load and reduced heat pump efficiency, leading to higher overall energy consumption.

The effectiveness of the operational improvements was quantified by analyzing changes in setpoint temperatures and nighttime operation. The average cooling setpoint increased from 24.7 °C to 25.2 °C (+0.5 °C), while the average heating setpoint decreased from 24.8 °C to 23.9 °C (−0.9 °C), indicating a shift toward more energy-efficient temperature settings. Nighttime unintended operation was reduced by a total of 2987 operating hours. Compared with the total annual operating time of 161,590 h, this corresponds to an overall reduction of approximately 1.8%. From a contribution perspective, this 1.8% reduction can be attributed to the elimination of unintended nighttime operation, whereas the remaining 11.1% of the total energy reduction is primarily associated with the optimization of setpoint temperatures. It should be noted that no feedback loops or auditing processes were implemented in this study. The improvements were achieved solely by applying operational constraints through existing controller settings. As no additional equipment or system modification was required, the implementation cost of these measures is considered negligible.

3.5. Operational efficiency analysis of representative systems before and after operational improvements

This section examines changes in representative systems before and after the implementation of energy conservation measures. Fig. 25 illustrates the changes in cooling temperature settings in the 5th-floor interaction space. Before the countermeasure, many setpoints were below 24 °C; however, after the countermeasure, most settings were adjusted to 25 °C or higher.

Fig. 26 presents the PLR and normalized COP before and after the countermeasures. Prior to the countermeasure, the average PLR was 0.38 and the average normalized COP was 1.09. After the countermeasure, the set temperature was raised, reducing the cooling load and resulting in a lower average PLR of 0.27. Despite this decrease in PLR, the average normalized COP remained unchanged at 1.09. This behavior

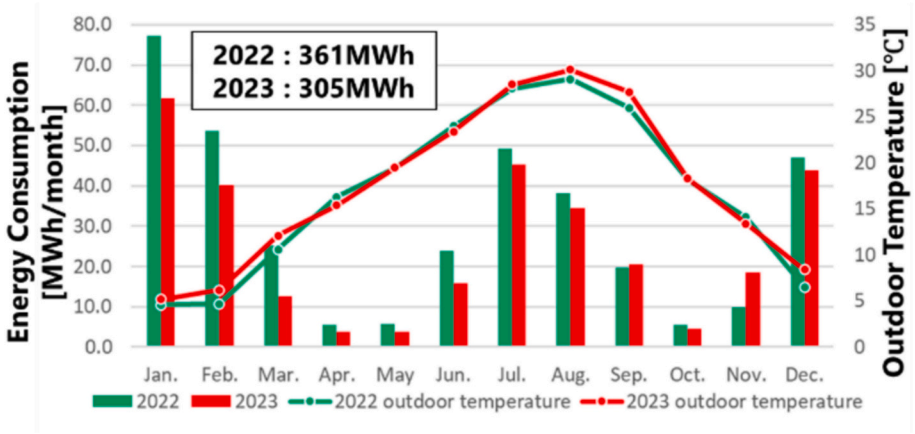

Fig. 24. Change in energy consumption for all systems.

Table 5
Results of outdoor temperature correction simulation.

	2022 Actual value	2023 Actual value	2023 Simulation value
Energy consumption (MWh)	361	305	314
Reduction rate (%)	–	15.4	12.9

can be explained by the pattern of the PLR distribution. COP decreases significantly when the PLR becomes very low (PLR < 0.20). In 2023, the amount of operation in this low-load region increased slightly, and this created a tendency for COP to decrease. On the other hand, COP also decreases when the PLR becomes high (PLR > 0.60). In 2023, the frequency of operation in this high-load region became smaller, and this created a tendency for COP to increase. These two effects — the increase in very low-load operation and the decrease in high-load operation — occurred at the same time. As a result, the annual average COP stayed nearly the same.

Next, the set temperature, PLR, and normalized COP during cooling before and after the countermeasures for the 5th-floor lecture rooms are shown in Figs. 27 and 28, respectively. The temperature setting similarly improved to 25 °C or higher. The PLR was 0.16 before the countermeasure but decreased to 0.13 after the countermeasure due to the smaller load. The normalized COP remained unchanged before and after the countermeasure.

Finally, the results for the 10th-floor faculty office are shown in Figs. 29 and 30. No significant changes in temperature setting, PLR, or normalized COP were observed for this room, as restrictions could not be imposed due to faculty preferences.

3.6. Simulation of capacity optimization

Although system overcapacity and low part-load operation have been repeatedly identified as major causes of efficiency degradation in VRF systems, most previous field studies have primarily reported their occurrence without quantitatively linking oversizing to COP degradation or evaluating the potential for efficiency recovery through capacity optimization. Consequently, many VRF systems at the Minoh Campus operate at low part-load ratios (PLRs), resulting in reduced efficiency.

To understand the underlying causes of these low PLRs, we first reviewed the load calculation sheets for the representative systems. As summarized in Table 6, commonly used design values were applied for occupant density, lighting load, equipment load, and outdoor air intake. These settings do not indicate any specific equipment-related factors that would inherently lead to excessive loads. However, while the load calculations assume that all rooms are simultaneously occupied at their maximum design population, the operational data in Fig. 18 show that many lecture rooms and laboratories remain unoccupied for extended periods. This discrepancy between design assumptions and actual usage patterns is considered a major reason why the actual load factors are significantly lower than the calculated design loads.

Although VRF systems allow indoor-unit-to-outdoor-unit connection capacity ratios exceeding 100%, this design allowance does not necessarily ensure that the installed outdoor-unit capacity is appropriately matched to actual operational conditions. The present results therefore suggest that the observed low load factors are not only a consequence of

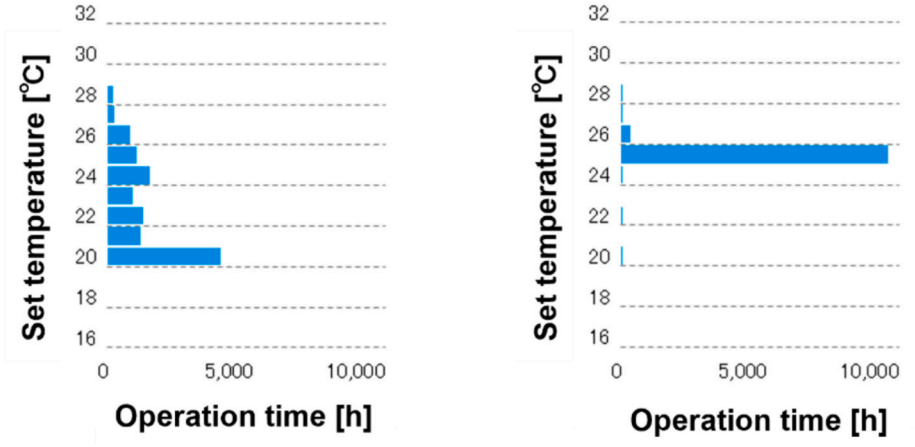

Fig. 25. Frequency distribution of set temperature for 5th floor interaction space.

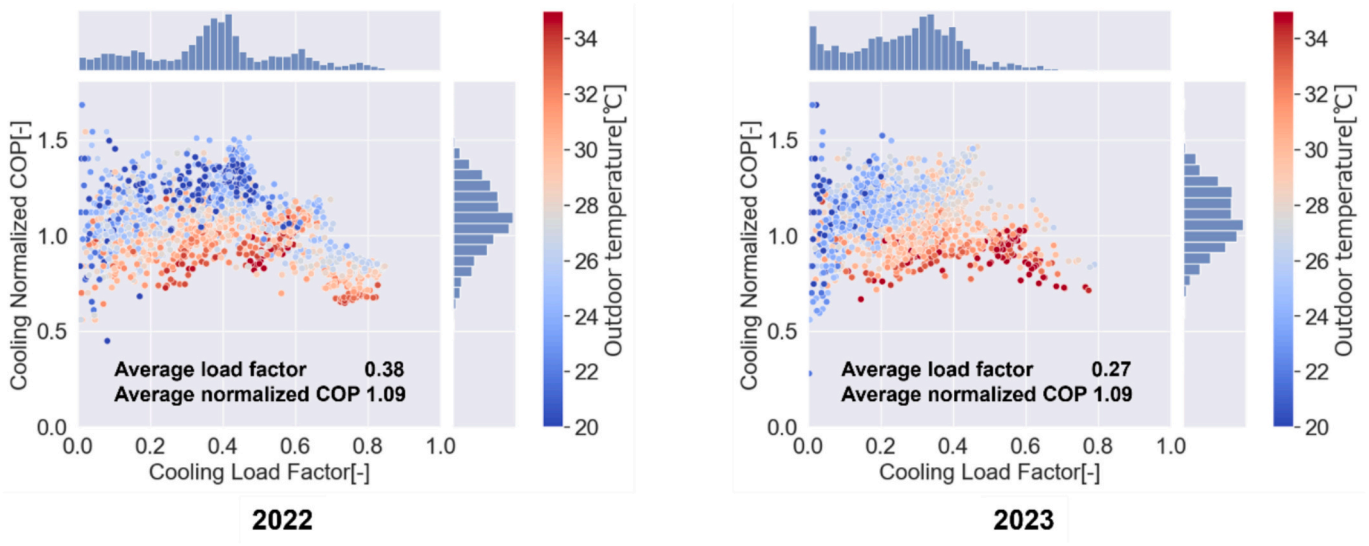

Fig. 26. Relationship between PLR and normalized COP for 5th floor interaction space.

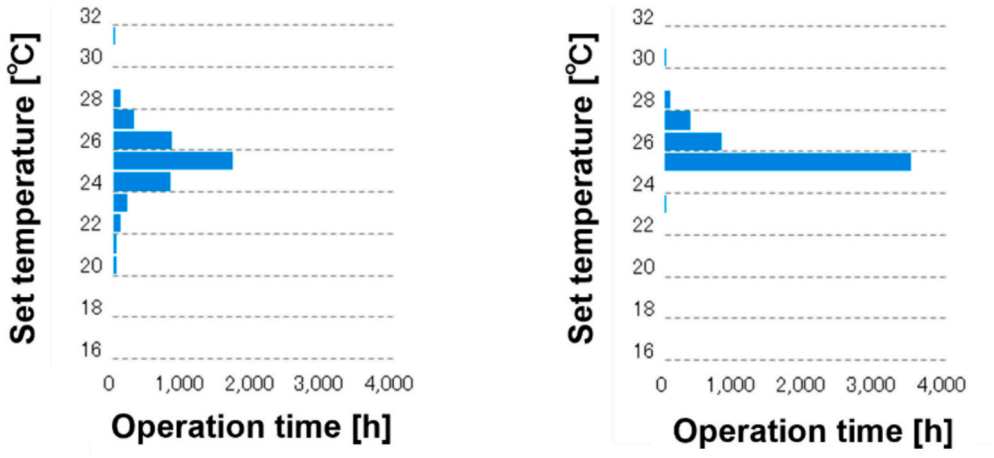

Fig. 27. Frequency distribution of set temperature for 5th floor lecture room.

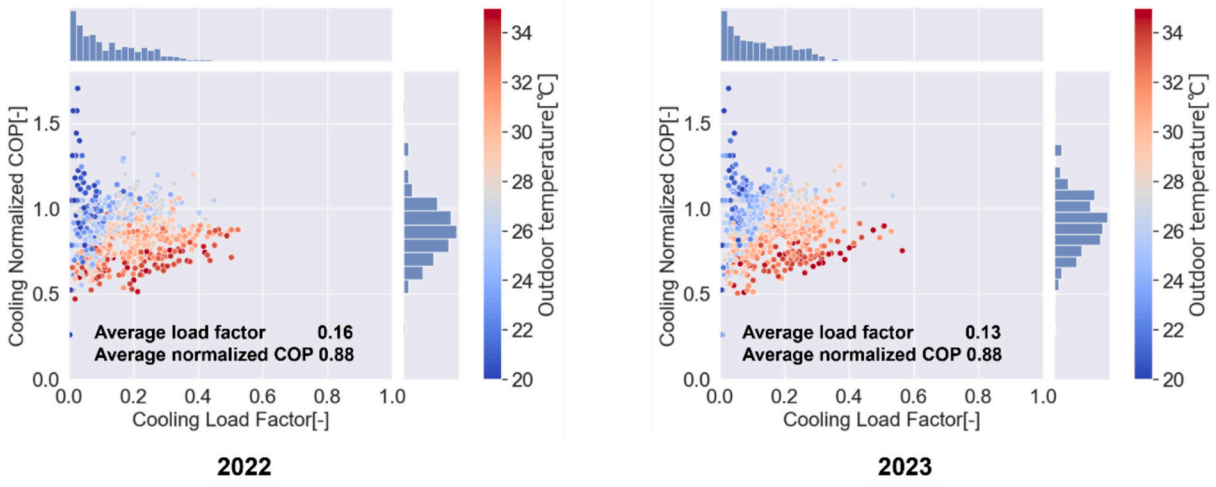

Fig. 28. Relationship between PLR and normalized COP for the 5th floor lecture room.

operational behavior, but also reflect systematic oversizing of outdoor units based on conservative design assumptions, indicating that outdoor-unit capacity can be reduced without compromising operational performance under realistic usage conditions.

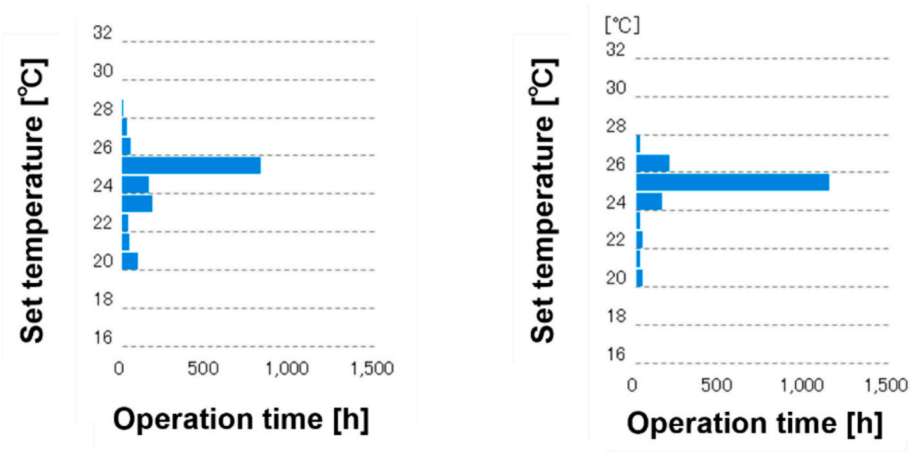

Fig. 29. Frequency distribution of set temperature for the 10th floor faculty office.

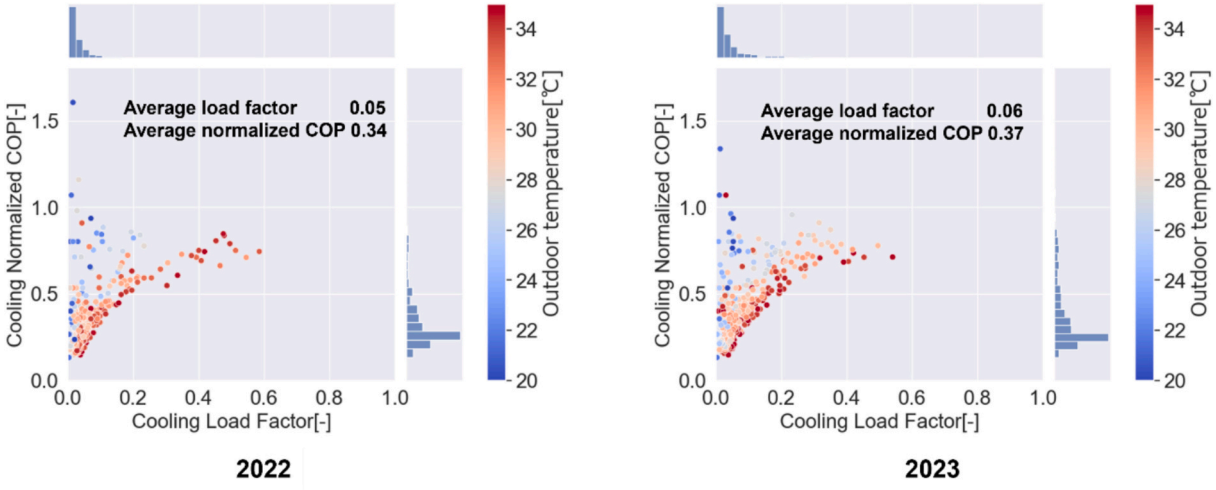

Fig. 30. Relationship between PLR and normalized COP for the 10th floor faculty office.

Table 6
The load calculation sheets for the representative systems.

		5th-floor interaction space	5th-floor lecture room	10th-floor faculty office
Building envelope heat load	W	7269	1865	952
Occupant density	Person/㎡	0.25	0.66	0.1
Lighting load	W/㎡	10	10	10
Equipment load	W/㎡	20	20	20
Outdoor air volume	CMH/person	30	30	30
Total load	W/m2	138	281	163
Design load	W/m2	144	284	172

Given the consistently low PLRs observed on campus, we conducted a simulation using 2023 operational data to evaluate the potential for improving system efficiency through outdoor unit (OU) capacity optimization (see Appendix A, Table A2). To illustrate this method, we selected the 5th-floor lecture room system, which exhibited a moderate PLR relative to the other representative systems.

Fig. 31 shows the relationship between PLR and COP, from which the approximation curves A = f(Xc) for cooling and B = g(Xh) for heating were derived. The maximum observed PLRs were 0.65 for cooling and 0.46 for heating, suggesting that the installed capacity could theoretically be reduced to 0.65 of its current value. Using this assumption, new approximation curves $A' = f(Xc / 0.65)$ and $B' = g(Xh / 0.65)$ were generated. The system capacity was then scaled by 1/0.65, and corrected power consumption values were calculated for all generated PLRs.

The results indicate that COP improved in the low-PLR regions—which occur more frequently—although some reduction was observed in the higher PLR range. Overall, the estimated energy reduction rates were 9.1% for cooling and 14.6% for heating (Table 7).

Approximate formulas were developed individually for all systems, and the aggregated results are presented in Table 8. Capacity optimization of the low-load systems was predicted to reduce energy consumption by 13.7% for cooling and 17.4% for heating, resulting in a total reduction of 15.9%. On average, the OU cooling capacity could be reduced by 31.4%.

The distribution of power reductions and reduction ratios for each system is shown in Fig. 32. As expected, the top four systems with the largest power reductions were the faculty offices with low PLRs, and the fifth was the guard room, which operates 24 h/day. The 5th-floor lecture room had a medium PLR and ranked 48th out of 100 in terms of energy savings, which was also moderate, as expected.

The above estimation results are based on actual operational conditions for capacity optimization. However, it is difficult to implement

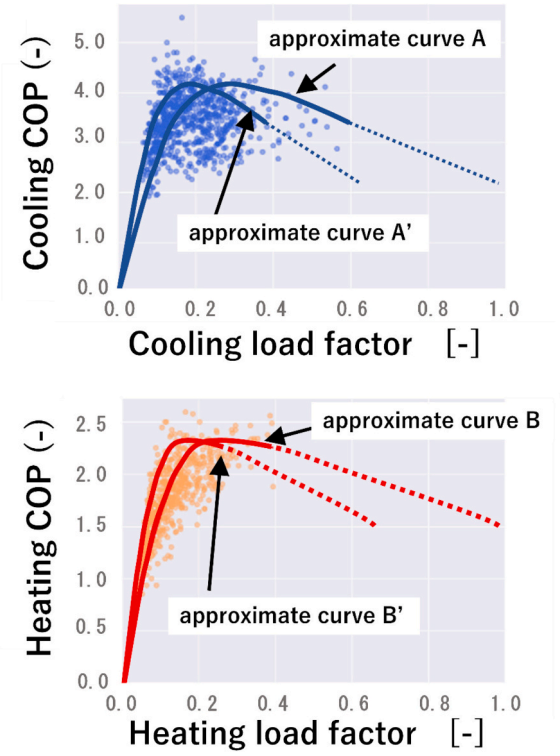

Fig. 31. Approximate curve of the 5th floor lecture room system (top: cooling, bottom: heating).

Table 7
Capacity optimization simulation results for the 5th-floor lecture room.

		Current condition	Simulation value	Reduction rate
Power consumption [kWh]	Cooling	1886	1714	9.1%
	Heating	2080	1776	14.6%
	Total	3966	3489	12.0%
OU cooling capacity [kW]		50	32.5	35.0%

Table 8
Capacity optimization simulation results for all systems.

		Current condition	Simulation value	Reduction rate
Power consumption [kWh]	Cooling	160.8	138.7	13.7%
	Heating	215.5	177.9	17.4%
	Total	376.3	316.6	15.9%
OU cooling capacity [kW]		4274.0	2932.1	31.4%

the same measures in other buildings because their actual operational status is unknown. Therefore, these results reflect only the maximum potential effect until the operational status becomes clear. Nevertheless, the findings suggest that energy savings are achievable without changing the operation method by optimizing VRF system capacity at the initial design stage.

The results of this study are broadly consistent with previous research on VRF performance. For example, Zhang et al. [16] observed that low partial-load operation substantially reduced system efficiency in office buildings, which is comparable to the low PLRs and reduced COP we identified in faculty offices at the Minoh Campus. Similarly, Liu et al. [18] reported that part-load operation was common in residential VRF systems, a trend also confirmed in our dataset across classrooms and faculty offices. These findings reinforce the conclusion that partial-load operation is a key determinant of VRF inefficiency across building types.

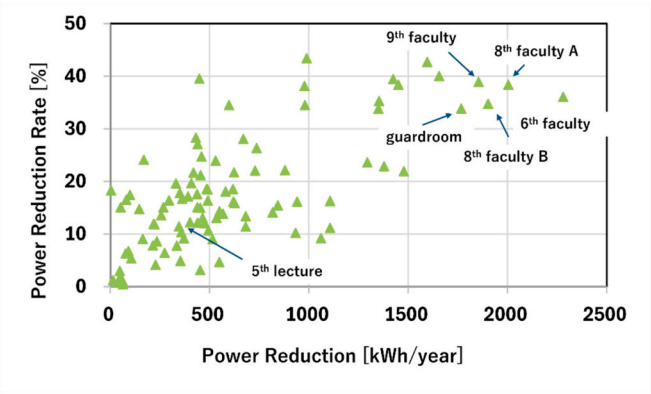

Fig. 32. Distribution of power reductions and reduction ratios.

At the same time, our study extends the literature by evaluating a much larger system scale—100 outdoor units and 650 indoor units—across a multi-purpose educational facility. Unlike prior studies that primarily focused on small-scale office or residential applications, the present work quantifies the combined impacts of user behavior, unattended operation, and oversized capacity. Moreover, by simulating capacity optimization, we provide evidence of a potential 15.9% energy reduction, which has not been explicitly quantified in earlier field studies. This underscores both the generalizability of existing findings and the novel contributions of our research to large-scale VRF system management.

4. Conclusion

This study presented a comprehensive field-based evaluation of the operational performance of a large-scale VRF system installed in a multi-purpose university building at Osaka University's Minoh Campus. Based on one year of high-resolution operational data from 100 outdoor units and 650 indoor units, the study yielded the following main conclusions.

First, based on one of the largest field datasets for a VRF system in a university building, this study demonstrated that VRF operational characteristics and performance vary substantially across typical academic space types.

- In lecture rooms and classrooms, intermittent and schedule-driven occupancy creates long periods without air-conditioning operation, resulting in frequent operation at extremely low part-load ratios (PLRs).
- In faculty offices, indoor units often operate in isolation and irregularly, further intensifying low-load operating conditions.
- In interaction spaces, where multiple indoor units operate concurrently, relatively higher PLRs are maintained, leading to higher normalized COPs.

These findings indicate that prolonged low-load operation in university buildings is not an exceptional phenomenon but a structural consequence of educational and research space usage, and that VRF system performance is governed more strongly by actual space-use patterns than by equipment specifications.

Second, this study quantitatively demonstrated user-induced operational inefficiencies and the effectiveness of practical operational improvement measures.

- Analysis of remote-controller operation revealed widespread excessive setpoint settings and unintended nighttime operation across academic spaces.

- Practical operational measures were implemented, including restricting extreme cooling and heating setpoints and enforcing automatic nighttime shutdown while allowing user operation during occupied periods.
- These measures reduced annual VRF energy consumption by 12.9% after correcting for outdoor temperature differences.

The results indicate that unrestricted manual control alone is insufficient in large university buildings, and that VRF systems require control frameworks that permit user operation while automatically restoring appropriate setpoints and operating states to suppress persistent user-driven inefficiencies.

Third, the study linked operational analysis results to design-level implications through capacity optimization.

- Long-term operational data revealed a systematic mismatch between conventional design assumptions based on simultaneous full occupancy and actual university usage.
- Although VRF systems allow indoor-unit-to-outdoor-unit connection capacity ratios exceeding 100%, outdoor-unit capacity was found to be reducible without compromising operational performance.
- Capacity optimization simulations based on observed PLR–COP relationships showed that downsizing outdoor-unit capacity could achieve an additional 15.9% reduction in energy consumption, with an average potential capacity reduction of approximately 30%.

These findings provide quantitative support for VRF design approaches that exploit connection diversity and reflect realistic educational building usage rather than conservative peak-load assumptions.

Overall, the results demonstrate that VRF system efficiency in large university buildings cannot be adequately evaluated or improved based solely on design specifications or short-term testing. Long-term field data are essential for revealing how educational space usage, user-driven operation, and system sizing interact to degrade performance. While the quantitative results are specific to the investigated campus, the underlying issues—intermittent classroom use, excessive reliance on manual control, and conservative capacity design—are common in university and other institutional buildings employing individually distributed air-conditioning systems. Therefore, the integrated approach presented in this study, combining large-scale operational analysis, explicit identification of user-induced inefficiencies, and capacity optimization that exploits allowable connection diversity, provides a practical and transferable framework for improving VRF performance in real educational facilities.

Nevertheless, several limitations of this study should be acknowledged. First, although high-resolution operational data were used, measurement noise and occasional data loss in the logging system cannot be completely avoided. Second, internal heat gains from occupants, lighting, and equipment were not directly measured and were therefore evaluated indirectly through operational behavior. Third, detailed partial occupancy information at the room level was not available, which limits the ability to fully separate occupancy effects from user-driven operational behavior. Future work should address these limitations by integrating occupancy sensing, predictive maintenance techniques based on long-term operational data, and automated setpoint optimization frameworks. In addition, further development of VRF control logic that balances user flexibility with automated restoration of efficient operating states represents a key direction for enhancing system efficiency in educational buildings.

CRediT authorship contribution statement

Toshihiro Suzuki: Writing – original draft, Validation, Methodology, Formal analysis, Conceptualization. **Yoshiyuki Shimoda:** Supervision, Project administration, Conceptualization. **Shuta Matsuura:** Visualization, Validation, Software, Formal analysis, Data curation. **Sumio Shiochi:** Writing – review & editing, Supervision, Conceptualization.

Declaration of competing interest

The authors declare that they have no known competing financial interests or personal relationships that could have appeared to influence the work reported in this paper.

Appendix A. Appendix A – Simulation method

Table A1
Method for outdoor temperature correction simulation.

1.	Use only weekday 2023 data in the simulation, considering that the use of the campus differs between weekdays and weekends. Simulate energy consumption if the outdoor temperature in 2023 is equal to that in 2022.
2.	Create a scatter plot showing the relationship between average daily outdoor temperature and daily energy consumption by cooling and heating. Create approximate functions for cooling and heating from the scatter plots using the following equations.
3.	$Cooling: ae^{bx} + c$ $Heating: ae^{-bx} + c$

As an example, Fig. A1 shows the relationship between outdoor temperature and power consumption on the 5th floor interaction space in 2022 and 2023. The approximate functions decreased due to the measures, and energy efficiency improved.

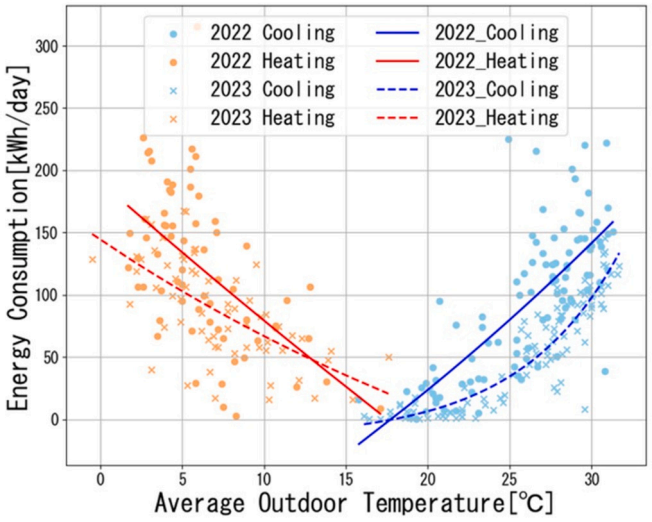

Fig. A1. Example of outdoor temperature correction for the 5th floor interaction space.

Table A2
Method for capacity optimization simulation.

1.	Use only data with OU operating time of ≥15 min in 2023; data with shorter operation times have large errors.
2.	Create a scatter plot showing the relationship between PLR and COP. Create an approximate curve from the scatter plots using second-order spline regression.
3.	Cooling: $A = f(Xc)$ Heating: $B = g(Xh)$
4.	Check the maximum PLR in the subject system. For that maximum PLR, create approximate curves $A' = f(Xc\ /\ X\_max)$ and $B' = g(Xh\ /\ X\_max)$, assuming that capacity can be reduced to the greater of cooling or heating (X_max = Max(Xc_max, Xh_max)). Calculate the COP correction and power consumption correction values for each system.
5.	COP Correction Value (Xc) = Measured COP(Xc) × A' / A Power Consumption Correction Value = ΣMeasured load throughput / Xc

Appendix B. Appendix B – List of Abbreviations.

Abbreviation	Full term	Description
VRF	Variable Refrigerant Flow	An air-conditioning system with variable refrigerant flow, connecting an outdoor unit with multiple indoor units via refrigerant piping to adjust cooling and heating capacity.
OU	Outdoor Unit	Unit installed outdoors that compresses/expands refrigerant and exchanges heat with the outside air via a heat exchanger.
IU	Indoor Unit	Unit installed indoors that exchanges heat between indoor air and refrigerant to control room temperature.
COP	Coefficient of Performance	A performance index calculated by dividing the cooling/heating capacity by the power consumption.
CC method	Compressor Curve method	A capacity calculation method using the compressor performance curve, based on actual operating refrigerant mass flow and enthalpy difference.
Qc	Cooling Capacity	Cooling capacity calculated from the indoor unit refrigerant mass flow and enthalpy difference.
Qh	Heating Capacity	Heating capacity calculated by adding the indoor unit fan power to the cooling capacity equation.
Wi	Indoor Unit Fan Power	Power consumption of the indoor unit fan, added or subtracted from the capacity calculation.
G	Refrigerant Mass Flow Rate	The mass flow rate of refrigerant, a key parameter for capacity calculation.
Δi	Enthalpy Difference	The difference in refrigerant enthalpy between the inlet and outlet of the indoor unit.
QVRF	VRF System Capacity	The total cooling/heating capacity of the VRF system.
P	Power Consumption	Electrical power consumed by equipment or systems.
RMSE	Root Mean Square Error	An error metric for regression models and correlation evaluation.
IU compressor-on ratio	Compressor-on Ratio of Indoor Unit	Ratio of compressor operation time to total operating time for the indoor unit.
kW	Kilowatt	A unit of power (1 kW = 1000 W).
MWh	Megawatt-hour	A unit of energy (1 MWh = 1000 kWh).
°C	Degree Celsius	A unit of temperature in the Celsius scale.

Appendix C. Appendix C – List of OUs.

No.	Model type	Number of IUs	Rated capacity (kW)	Rated input (kW)	Installed floor

(*continued on next page*)

(*continued*)

No.	Model type	Number of IUs	Rated capacity (kW)		Rated input (kW)		Installed floor
			cooling	heating	cooling	heating	
			cooling	heating	cooling	heating	
1	RXUP500F	8	50.0	56.0	13.1	13.9	7
2	RXUP224F	6	22.4	25.0	5.41	5.82	7
3	RXUP560F	10	56.0	63.0	15.7	16.5	7
4	RXUP280F	3	28.0	31.5	7.84	8.24	7
5	RXUP400F	5	40.0	45.0	10.7	10.9	7
6	RXUP400F	10	40.0	45.0	10.7	10.9	8
7	RXUP280F	7	28.0	31.5	7.84	8.24	8
8	RXUP400F	8	40.0	45.0	10.7	10.9	8
9	RXUP400F	8	40.0	45.0	10.7	10.9	8
10	RXUP400F	10	40.0	45.0	10.7	10.9	9
11	RXUP280F	7	28.0	31.5	7.84	8.24	9
12	RXUP400F	8	40.0	45.0	10.7	10.9	9
13	RXUP400F	8	40.0	45.0	10.7	10.9	9
14	RXUP560F	5	56.0	63.0	15.7	16.5	5
15	RXUP450F	10	45.0	50.0	12.6	12.4	10
16	RXUP400F	7	40.0	45.0	10.7	10.9	10
17	RXUP280F	7	28.0	31.5	7.84	8.24	10
18	RXUP400F	8	40.0	45.0	10.7	10.9	10
19	RXUP400F	8	40.0	45.0	10.7	10.9	10
20	RXUP560F	5	56.0	63.0	15.7	16.5	1
21	RXUP280F	5	28.0	31.5	7.84	8.24	1
22	RXUP280F	6	28.0	31.5	7.84	8.24	2
23	RXUP280F	4	28.0	31.5	7.84	8.24	2
24	RXUP670F	13	67.0	77.5	17.9	23.1	2
25	RXUP560F	8	56.0	63.0	15.7	16.5	5
26	RXUP560F	8	56.0	63.0	15.7	16.5	5
27	RXUP224F	4	22.4	25.0	5.41	5.82	5
28	RXUP280F	4	28.0	31.5	7.84	8.24	5
29	RXUP560F	8	56.0	63.0	15.7	16.5	5
30	RXUP560F	8	56.0	63.0	15.7	16.5	6
31	RXUP560F	8	56.0	63.0	15.7	16.5	6
32	RXUP615F	8	61.5	69.0	16.8	19.1	6
33	RXUP900F	9	90.0	100.0	25.2	24.8	6
34	RXUP900F	9	90.0	100.0	25.2	24.8	1
35	REUP560D	14	56.0	63.0	16.5	17.1	1
36	RXUP224F	5	22.4	25.0	5.41	5.82	1
37	RXUP335F	8	33.5	37.5	8.91	10.8	1
38	RXUP224F	3	22.4	25.0	5.41	5.82	1
39	RXUP615F	10	61.5	69.0	16.8	19.1	1
40	RXUP335F	9	33.5	37.5	8.91	10.8	2
41	RXUP775F	7	77.5	90.0	21	24.6	2
42	RXUP560F	8	56.0	63.0	15.7	16.5	2
43	RXUP224F	4	22.4	25.0	5.41	5.82	5
44	RXUP560F	8	56.0	63.0	15.7	16.5	5
45	RXUP280F	4	28.0	31.5	7.84	8.24	5
46	RXUP224F	3	22.4	25.0	5.41	5.82	5
47	RXUP670F	8	67.0	77.5	17.9	23.1	5
48	RXUP670F	8	67.0	77.5	17.9	23.1	5
49	RXUP560F	8	56.0	63.0	15.7	16.5	5
50	RXUP560F	6	56.0	63.0	15.7	16.5	5
51	RXUP615F	8	61.5	69.0	16.8	19.1	6
52	RXUP670F	8	67.0	77.5	17.9	23.1	6
53	RXUP670F	8	67.0	77.5	17.9	23.1	6
54	RXUP500F	13	50.0	56.0	13.1	13.9	6
55	RXUP500F	9	50.0	56.0	13.1	13.9	7
56	RXUP670F	6	67.0	77.5	17.9	23.1	7
57	RXUP400F	8	40.0	45.0	10.7	10.9	7
58	RXUP224F	4	22.4	25.0	5.41	5.82	7
59	SZVYCP450K	1	40.0	45.0	16.9	14.9	1
60	SZVYCP450K	1	40.0	45.0	16.9	14.9	1
61	SZVYCP140K	1	14.0	16.0	3.31	3.71	1
62	RXUP450F	10	45.0	50.0	12.6	12.4	8
63	RXUP450F	8	45.0	50.0	12.6	12.4	8
64	RXUP450F	8	45.0	50.0	12.6	12.4	8
65	RXUP400F	7	40.0	45.0	10.7	10.9	8
66	RXUP335F	7	33.5	37.5	8.91	10.8	8
67	RXUP450F	10	45.0	50.0	12.6	12.4	9
68	RXUP450F	8	45.0	50.0	12.6	12.4	9
69	RXUP450F	8	45.0	50.0	12.6	12.4	9
70	RXUP400F	7	40.0	45.0	10.7	10.9	9
71	RXUP280F	7	28.0	31.5	7.84	8.24	9
72	RXUP335F	2	33.5	37.5	8.91	10.8	5

(*continued on next page*)

(*continued*)

No.	Model type	Number of IUs	Rated capacity (kW)		Rated input (kW)		Installed floor
			cooling	heating	cooling	heating	
73	RXUP500F	10	50.0	56.0	13.1	13.9	10
74	RXUP560F	8	56.0	63.0	15.7	16.5	10
75	RXUP560F	8	56.0	63.0	15.7	16.5	10
76	RXUP280F	7	28.0	31.5	7.84	8.24	10
77	RXYP335FA	2	33.5	37.5	10.4	11.2	3
78	RXUP335F	5	33.5	37.5	8.91	10.8	3
79	RXUP450F	6	45.0	50.0	12.6	12.4	3
80	RXUP450F	6	45.0	50.0	12.6	12.4	3
81	RXUP450F	6	45.0	50.0	12.6	12.4	3
82	RXUP560F	8	56.0	63.0	15.7	16.5	3
83	RXUP335F	4	33.5	37.5	8.91	10.8	3
84	RXYP730FA	5	73.0	82.5	24.9	25.9	3
85	RXUP560F	4	56.0	63.0	15.7	16.5	3
86	RXUP224F	4	22.4	25.0	5.41	5.82	4
87	RXUP224F	4	22.4	25.0	5.41	5.82	4
88	RXUP224F	4	22.4	25.0	5.41	5.82	4
89	RXUP224F	4	22.4	25.0	5.41	5.82	4
90	RXUP224F	4	22.4	25.0	5.41	5.82	4
91	RXUP224F	4	22.4	25.0	5.41	5.82	4
92	RXYP1360F	5	136.0	150.0	45.4	48.9	4
93	RXUP224F	3	22.4	25.0	5.41	5.82	4
94	RXUP224F	4	22.4	25.0	5.41	5.82	4
95	RXUP224F	8	22.4	25.0	5.41	5.82	4
96	RXUP224F	8	22.4	25.0	5.41	5.82	4
97	RXUP224F	4	22.4	25.0	5.41	5.82	4
98	SZVCP224K	1	20.0	–	6.09	–	4
99	SZVCP224K	1	20.0	–	6.09	–	4
100	SZVCP224K	1	20.0	–	6.09	–	4
sum		650	4275	4740	1188	1252	–

Data availability

Data will be made available on request.

References

[1] IEA, World Energy Outlook, IEA, Paris, 2022 https://www.iea.org/reports/world-energy-outlook-2022, 2022. accessed 5 October 2024.

[2] M.A. Abdulhussain, CFD pretending of vapor and liquid refrigerant mixing in variable speed scroll compressor, Eng. Sci. Technol. Int. J. 22 (2019) 168–176, https://doi.org/10.1016/j.jestch.2018.07.017.

[3] S. Ham, S. Choi, J.H. Jeong, Two-phase flow distribution in a refrigerant distributor having four IU connections of a variable refrigerant flow system, Int. J. Refrig. 126 (2021) 246–258, https://doi.org/10.1016/j.ijrefrig.2021.01.014.

[4] A.G. Devecioğlu, V. Oruç, Energetic performance analysis of R466A as an alternative to R410A in VRF systems, Eng. Sci. Technol. Int. J. 23 (2020) 1425–1433, https://doi.org/10.1016/j.jestch.2020.04.003.

[5] D. Kim, H. Cho, J. Koh, P. Im, Net-zero energy building design and life-cycle cost analysis with air-source variable refrigerant flow and distributed photovoltaic systems, Renew. Sust. Energ. Rev. 118 (2020) 109508, https://doi.org/10.1016/j.rser.2019.109508.

[6] H.C. Chuang, M.L. Guo, Z.H. Liao, C.T. Lee, Double-feedback control with stepless variable speed driving technology by sensing refrigerant pressure and indoor temperature applied to air conditioning system, Energ. Buildings 218 (2020) 110053, https://doi.org/10.1016/j.enbuild.2020.110053.

[7] B. Pandey, B. Bohara, R. Pungaliya, S.C. Patwardhan, R. Banerjee, A thermal comfort-driven model predictive controller for residential split air conditioner, J. Build. Eng. 42 (2021) 102513, https://doi.org/10.1016/j.jobe.2021.102513.

[8] C. Liu, T. Zhao, J. Zhang, T. Chen, X. Li, M. Xu, X. Yang, Operational electricity consumption analyze of VRF air conditioning system and centralized air conditioning system based on building energy monitoring and management system, Procedia Eng. 121 (2015) 1856–1863, https://doi.org/10.1016/j.proeng.2015.09.167.

[9] J. Liu, J. Wang, G. Li, H. Chen, L. Shen, L. Xing, Evaluation of the energy performance of variable refrigerant flow systems using dynamic energy benchmarks based on data mining techniques, Appl. Energy 208 (2017) 522–539, https://doi.org/10.1016/j.apenergy.2017.09.116.

[10] Y. Guo, H. Chen, Fault diagnosis of VRF air-conditioning system based on improved Gaussian mixture model with PCA approach, Int. J. Refrig. 118 (2020) 1–11, https://doi.org/10.1016/j.ijrefrig.2020.06.009.

[11] Z. Zhou, G. Li, H. Chen, H. Zhong, Fault diagnosis method for building VRF system based on convolutional neural network: considering system defrosting process and sensor fault coupling, Build. Environ. 195 (2021) 107775, https://doi.org/10.1016/j.buildenv.2021.107775.

[12] Y.P. Zhou, J.Y. Wu, R.Z. Wang, S. Shiochi, Energy simulation in the variable refrigerant flow air-conditioning system under cooling conditions, Energ. Buildings 39 (2007) 212–220, https://doi.org/10.1016/j.enbuild.2006.06.005.

[13] R. Zhang, K. Sun, T. Hong, Y. Yura, R. Hinokuma, A novel variable refrigerant flow (VRF) heat recovery system model: development and validation, Energ. Buildings 168 (2018) 399–412, https://doi.org/10.1016/j.enbuild.2018.03.028.

[14] D. Kim, S.J. Cox, H. Cho, P. Im, Evaluation of energy savings potential of variable refrigerant flow (VRF) from variable air volume (VAV) in the U.S. climate locations, Energy Rep. 3 (2017) 85–93, https://doi.org/10.1016/j.egyr.2017.05.002.

[15] J. Li, H. Li, Y. Guo, J. Lu, Z. Zhang, J. Zhu, Energy consumption analysis and operating characteristics research on small time scale of variable refrigerant flow air conditioning systems in public buildings, Therm. Sci. Eng. Prog. 55 (2024) 102937, https://doi.org/10.1016/j.tsep.2024.102937.

[16] G. Zhang, X. Li, W. Shi, B. Wang, Y. Cao, Influence of occupant behavior on the energy performance of variable refrigerant flow systems for office buildings: a case study, J. Build. Eng. 22 (2019) 327–334, https://doi.org/10.1016/j.jobe.2018.12.020.

[17] M. Qian, D. Yan, H. Liu, U. Berardi, Y. Liu, Power consumption and energy efficiency of VRF system based on large scale monitoring virtual sensors, Build. Simul. 13 (2020) 1145–1156, https://doi.org/10.1007/s12273-020-0670-x.

[18] H. Liu, Y. Wu, D. Yan, S. Hu, M. Qian, Investigation of VRF system cooling operation and performance in residential buildings based on a large-scale dataset, J. Build. Eng. 61 (2022) 105219, https://doi.org/10.1016/j.jobe.2022.105219.

[19] X. Zhou, N. Wang, J. Zou, G. Liu, X. Zhuang, G. Liu, Analysis and prediction of energy consumption in office buildings with variable refrigerant flow systems: a case study, Build. Eng. 97 (2024) 110936, https://doi.org/10.1016/j.jobe.2024.110936.

[20] Y. He, Q. Gong, Z. Zhou, H. Chen, Development of a hybrid VRF system energy consumption prediction model based on data partitioning and swarm intelligence algorithm, Build. Eng. 74 (2023) 106868, https://doi.org/10.1016/j.jobe.2023.106868.

[21] I. Kang, K. Ho Lee, J. Hyeon Lee, J. Woo Moon, Artificial neural network–based control of a variable refrigerant flow system in the cooling season, Energies 11 (7) (2018) 1643, https://doi.org/10.3390/en11071643.

[22] Y. Lee, W. Kim, Development of an optimal start control strategy for a variable refrigerant flow (VRF) system, Energies 14 (2) (2021) 271, https://doi.org/10.3390/en14020271.

[23] N. Es-sakali, Z. Zoubir, S.I. Kaitouni, M.O. Mghazli, M. Cherkaoui, J. Pfafferott, Advanced predictive maintenance and fault diagnosis strategy for enhanced HVAC efficiency in buildings, Appl. Therm. Eng. 254 (2024) 123910, https://doi.org/10.1016/j.applthermaleng.2024.123910.

[24] C. Ninagawa, IoT/AI Control of VRF Distributed Building air-Conditioners, Springer Singapore, 2024, https://doi.org/10.1007/978-981-99-9199-0.
[25] Daikin Industries, Ltd., D-NET Remote Monitoring Program, http://www.daikinac.com/content/the-daikin-difference/d-net-remote-monitoring-program/ (accessed 3 March, 2025.
[26] N. Sekine, Y. Furuhashi, S. Kametani, The simple performance evaluation method of VRF system using volumetric efficiency of compressor, in: International Refrigeration and Air Conditioning Conference, Purdue University, West Lafayette, 2012.